nature cell biology

ARTICLES

https://doi.org/10.1038/s41556-019-0376-4

The inner centromere is a biomolecular condensate scaffolded by the chromosomal passenger complex

Prasad Trivedi[1,2], Francesco Palomba[3], Ewa Niedzialkowska[2], Michelle A. Digman[3], Enrico Gratton[3] and P. Todd Stukenberg[1,2*]

The inner centromere is a region on every mitotic chromosome that enables specific biochemical reactions that underlie properties, such as the maintenance of cohesion, the regulation of kinetochores and the assembly of specialized chromatin, that can resist microtubule pulling forces. The chromosomal passenger complex (CPC) is abundantly localized to the inner centromeres and it is unclear whether it is involved in non-kinase activities that contribute to the generation of these unique chromatin properties. We find that the borealin subunit of the CPC drives phase separation of the CPC in vitro at concentrations that are below those found on the inner centromere. We also provide strong evidence that the CPC exists in a phase-separated state at the inner centromere. CPC phase separation is required for its inner-centromere localization and function during mitosis. We suggest that the CPC combines phase separation, kinase and histone code-reading activities to enable the formation of a chromatin body with unique biochemical activities at the inner centromere.

The chromatin region between sister centromeres, the inner centromere, is the region in which cohesion is retained until anaphase and that serves as the platform for mitotic signalling[1]. The inner centromere also has to be uniquely organized to withstand the pulling forces generated at kinetochores during mitosis[2,3]. The emergence of such properties requires compartmentalization of multiple biochemical reactions to this chromatin region. How such compartmentalization is achieved is an important unanswered question.

Phase separation is an emergent property of multivalent scaffold proteins that are present at high local concentration and display liquid-like behaviours. Phase separation underlies the formation of membraneless organelles and is able to compartmentalize various biochemical processes in both the cytoplasm and interphase nuclei[4–7]. We hypothesized that phase separation underlies compartmentalization at the inner centromeres. The CPC—which contains Aurora-B kinase and at least three other subunits, including INCENP, survivin and borealin—is an abundant component of the inner centromere (~10 μM)[8] and regulates most of its known functions[1].

Mitotic signalling is initiated by the concentration of the CPC on inner-centromeric chromatin or at the spindle midzone, which enables autoactivation of Aurora-B kinase[9–11]. During mitosis, the CPC is recruited to the inner centromere by two orthogonal histone marks—H3T3ph and H2AT120ph[12]. Survivin directly binds to H3T3ph and borealin indirectly binds to H2AT120ph through its interaction with SGO1[13–18]. However, it is unclear how the histone-reading subunit survivin could be an anchor as it has a turnover rate at inner centromeres that is around five times greater than the rates of Aurora-B, INCENP and borealin[19,20]. Furthermore, it is unclear how the weak affinity (~2–4 μM) between survivin and H3T3ph can stably anchor CPC[17,18]. Although this concern is alleviated by the involvement of a second histone mark, it is unclear how SGO1 could anchor most of the CPC as its concentration is around 5 times lower than the CPC subunits[21].

The kinase activity of Aurora-B has a well-appreciated role in regulating the inner centromere[1,22,23]. Recent evidence suggests that non-kinase subunits of the CPC protect cohesion at inner centromeres independent of their role in the localization of Aurora-B[24]. It is unclear how the non-kinase subunits of the CPC exert these effects on the biophysical organization of the inner centromere. Here we demonstrate that the inner-centromere-targeting region of the CPC can undergo phase separation in vitro, and we provide strong evidence that the CPC at the inner centromere exists in a phase-separated state. We also demonstrate that the ability of the CPC to undergo phase separation is important for its inner-centromere localization and function. We provide a model that explains how the combination of kinase, histone code-reading and phase-separation activities in a single complex enables the formation of an inner-centromere body at a single location of every chromosome at the beginning of mitosis.

Results

The centromere-targeting subunits of the CPC undergo phase separation in vitro. We tested whether subunits of the CPC could undergo phase separation in vitro. We expressed survivin, borealin and the 58 N-terminal amino acids of INCENP (which, together, we refer to as ISB) in *Escherichia coli* (Fig. 1a, Supplementary Fig. 1a,b). This set of proteins has all of the activities required to localize the CPC to the inner centromere[25]. We observed spontaneous ISB phase separation under conditions of high protein concentration, low salt concentration or the presence of the molecular crowding agent polyethylene glycol 3350 (PEG-3350; Fig. 1b–d). Coacervates formed from green fluorescent protein (GFP)-tagged

[1]Department of Cell Biology, University of Virginia, School of Medicine, Charlottesville, VA, USA. [2]Department of Biochemistry and Molecular Genetics, University of Virginia, School of Medicine, Charlottesville, VA, USA. [3]Laboratory of Fluorescence Dynamics, The Henry Samueli School of Engineering, University of California, Irvine, CA, USA. *e-mail: pts7h@virginia.edu

ISB were fluorescent, demonstrating that they are composed of CPC proteins (Fig. 1d). The homologous complex from *Xenopus laevis* also underwent phase separation (Supplementary Fig. 2a), demonstrating evolutionary conservation of this property.

The ISB coacervates display liquid-like properties that are similar to those observed in phase-separating proteins[4–6,26]. They are highly circular in shape, the larger coacervates undergo deformation upon application of shear stress by placement of a coverslip on them, and the coacervates undergo fusion at early time points after induction of phase separation (Fig. 1e, Supplementary Fig. 2b,c). Some proteins that undergo phase separation maintain their liquid-like state whereas others gelate over time[4]. We hypothesized that ISB formed a gel as no fusion events were seen (Fig. 1e) after around 1 min of inducing phase separation and we observed coacervates that appeared to be arrested mid-fusion (Supplementary Fig. 2j–l). We tested the material property of the ISB droplet by photobleaching a sub-region of GFP–ISB coacervate and saw little internal rearrangement over the time scale of a minute. We conclude that ISB coacervates quickly (~1 min) mature to have gel-like properties (Fig. 1f).

The size of ISB coacervates were dependent on concentrations of salt, ISB or molecular crowding agent (Supplementary Fig. 2d–i). These data suggest that charge-based intermolecular interactions between ISB molecules underlie coacervate formation. Interestingly, the ISB phase diagram predicts that the CPC would exist in a phase-separated state at concentrations that are estimated at the inner centromeres (10 μM), whereas it would exist in a homogeneous state at cytoplasmic CPC concentrations (0.01 μM)[8] under physiological conditions (Fig. 1g).

The dynamics of CPC subunits are similar in coacervates and at the inner centromere. To determine whether the ISB in the droplets exchanged with ISB in the surrounding buffer, we performed fluorescence recovery after photobleaching (FRAP) of GFP–ISB droplets in vitro. We observed a slow exchange of ISB protein ($t_{1/2}$ = 99.71 s, 50.86% mobile fraction; Fig. 2a,b, Supplementary Fig. 2m). Interestingly, these exchange dynamics are similar to what has been measured for INCENP at the inner centromeres in vivo ($t_{1/2}$ = 83.2 ± 33.5 s, ~55–60% mobile fraction)[27]. We also compared the diffusion rates of CPC components inside coacervates in vitro and at inner centromeres using fluorescence correlation spectroscopy (FCS). GFP–borealin dynamics in both the cytoplasm and the inner centromere is best described by a two-populations model (slow diffusing population, D_{slow} = 0.1–1 μm^2 s^{-1}; fast diffusing population, D_{fast} = 10–15 μm^2 s^{-1}) as previously reported[28,29] (Supplementary Fig. 3a–e). The slow diffusing population was previously interpreted as the diffusion of borealin as part of the CPC complex. The CPC in the inner centromere diffused slower than the CPC in the cytoplasm of mitotic cells (Fig. 2b,c). Interestingly, the CPC in the inner centromere (D_{slow} = 0.1–0.5 μm^2 s^{-1}) had a similar diffusion rate to that measured for GFP–INCENP inside the ISB droplet in vitro (D = 0.05–0.3 μm^2 s^{-1}; Fig. 2d,e, Supplementary Fig. 3f). ISB outside the droplet diffused much faster than inside the droplet (Fig. 2e), demonstrating that phase separation changes the hydrodynamic properties of the protein. ISB outside the coacervates diffused faster than the CPC in the cytoplasm (Fig. 2c,e), presumably because of the more crowded environment of the cytoplasm. Strong correlation between both FRAP and FCS data, in vitro and in vivo, demonstrates that coacervate formation may explain the reduced dynamics of the CPC components measured at inner centromeres, and suggests that the CPC exists as a coacervate inner centromeres.

ISB coacervates enrich inner-centromere components. The CPC is recruited to inner centromeres by multivalent interactions with at least three proteins—histone H3pT3, SGO1 and HP1α. The interactions that drive ISB coacervation may block the binding surfaces for other inner-centromere proteins. To test whether survivin in coacervates still binds to histone tails, we mixed fluorescent H3T3ph peptides with preformed ISB coacervates and observed the partition of these peptides. H3T3ph peptides were more enriched in coacervates than unphosphorylated peptides. Coacervates generated with ISB containing a survivin H3pT3-binding mutation (H80A) did not enrich H3pT3 compared with H3 peptides (Fig. 3a, Supplementary Fig. 4d). Thus, survivin retains the ability to 'read' the histone tails within coacervates. A key heterochromatin regulator, HP1α, controls CPC activity and localization in mitosis[30–32]. We mixed CF555-labelled HP1α with preformed ISB coacervates and observed robust enrichment of HP1α in ISB coacervates (Fig. 3b). We used conditions in which HP1α was unable to undergo phase separation on its own. SGO1 interacts with the borealin subunit of the CPC through its N terminus and drives its localization to the inner centromere[16]. We observed strong enrichment of CF555–hSGO1$^{1–112}$ in the ISB coacervates (Fig. 3c). By contrast, molecules that either do not interact with the CPC or are not components of the inner centromere, such as GFP, GFP–Mad2 or Cy3-azide, showed marginal or no enrichment in the ISB phase (Fig. 3g, Supplementary Fig. 4b,c). Thus, a number of inner-centromere regulators robustly interact with ISB in the droplet phase.

Another subassembly of the CPC, xAurora-B–xINCENP$^{790–847}$ also partitioned into the ISB coacervates (Fig. 3f), confirming previous results[33,34]. This observation provides evidence that the current models of autoactivation are compatible with phase separation because the kinase was not excluded from the droplet. Nucleic acids (α-satellite RNA and DNA) were enriched in ISB coacervates (Fig. 3d,e, Supplementary Fig. 4a). Surprisingly, coacervates also bound mononucleosomes independent of T3 phosphorylation, demonstrating that this simple assay can be used to identify new CPC activities.

α/β-Tubulin dimers were enriched in ISB coacervates (Supplementary Fig. 3e). Surprisingly, ISB coacervates nucleated microtubules at concentrations of α/β-tubulin dimers that are 20-fold below the critical concentration (Supplementary Fig. 3f), similar to what has been observed for centrosome proteins in *Caenorhabditis elegans*[26]. No microtubule nucleation was seen in the absence of ISB or GTP (Supplementary Fig. 3f). Interestingly, the CPC regulates microtubule formation near chromosomes, although this has been attributed to its ability to inhibit the microtubule depolymerase MCAK[35].

Inner-centromere components enhance phase separation of ISB. ISB spontaneously undergoes phase separation in physiological conditions at concentrations of around 6 μM, which is lower than the concentrations that are estimated to be present at the inner centromere (10 μM; Fig. 1g). However, the presence of other inner-centromere components or mitotic post-translational modifications might promote or inhibit phase separation. We observed that α-satellite DNA, histone H3.3 polynucleosomes, histone H3.1 mononucleosomes, H3T3ph mononucleosomes and microtubule bundles all induce phase separation under conditions in which ISB exists in a homogeneous phase on its own (Fig. 4a–c). Thus, a number of inner-centromere components promote the ISB phase separation.

HP1α can undergo phase separation and is a regulator of the CPC in the inner centromere. HP1α is phosphorylated on both its N terminus and hinge region during mitosis[36]. We measured the saturation concentration of the ISB in the presence and absence of HP1a by measuring the concentration of the ISB present in the homogenous phase after centrifugation. The saturation concentration of ISB was ~6 μM at physiological ionic strength, consistent with the phase diagram. Interestingly, phosphorylated HP1α promoted phase separation of ISB (reducing the saturation concentration of the ISB to ~3.5 μM), whereas the unphosphorylated HP1α

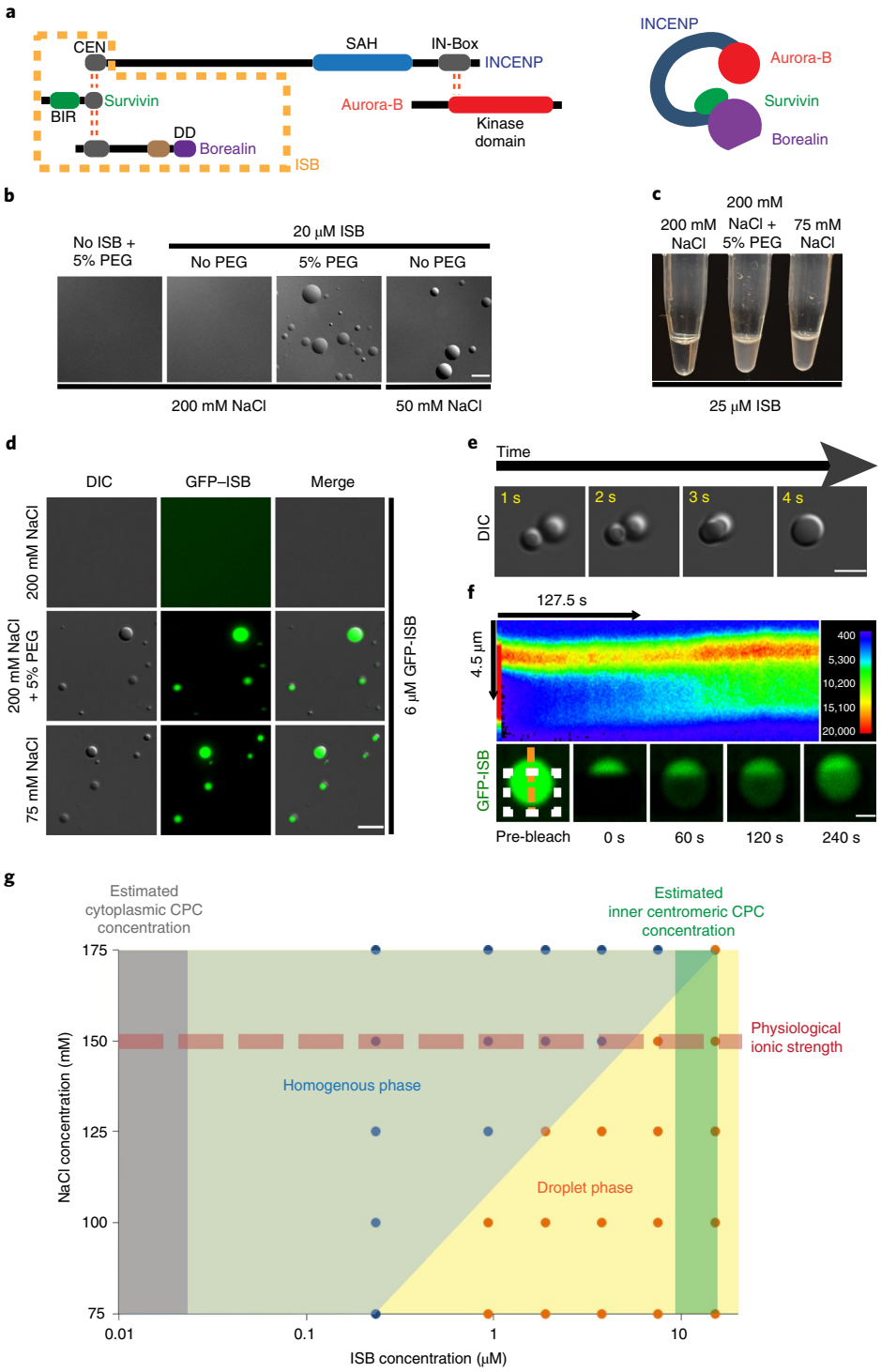

Fig. 1 | The centromere-targeting region of the CPC undergoes phase separation in vitro under physiological conditions. a, Schematic of the CPC showing various domains in the CPC subunits. DD, dimerization domain; BIR, baculovirus IAP repeat domain; CEN, centromere-targeting domain; SAH, single α-helix domain; IN-Box, INCENP conserved box. The red dotted lines indicate interactions between subunits. The orange dotted box indicates the ISB region used for biochemical analysis in this study. **b**, DIC micrographs of the ISB coacervates under the indicated conditions. PEG, PEG-3350. **c**, Turbidity generated by the phase separation of the ISB complex under the indicated conditions. **d**, The phase-separated droplets of the GFP–ISB complex contain fluorescence. **e**, Fusion of ISB coacervates as visualized by time-lapse imaging. **f**, FRAP analysis of GFP–ISB coacervates. GFP–INCENP$^{1-58}$ was photobleached in the ISB coacervates (the white dotted box indicates the bleached area) and the recovery of fluorescence was monitored. Top, a pseudo-coloured kymograph of the fluorescence intensity at the orange dotted line (shown at the bottom) of the FRAP experiment. Colour corresponds to the fluorescence intensity as indicated by the colour scale. Bottom, time-lapse images from the FRAP experiment. For **b**–**f**, the experiment was repeated independently three times. **g**, Phase diagram of ISB phase separation as a function of the concentration of NaCl and ISB. The red dotted line indicates conditions with physiological ionic strength. Blue (homogenous phase) and orange (droplet phase) circles show the actual conditions sampled in the experiment. The grey shaded region indicates the estimated cytoplasmic CPC concentration and the dark-green shaded region indicates estimated centromeric CPC concentration. For **b** and **d**–**f**, scale bars, 5 μm. Source data for **g** are provided in Supplementary Table 2.

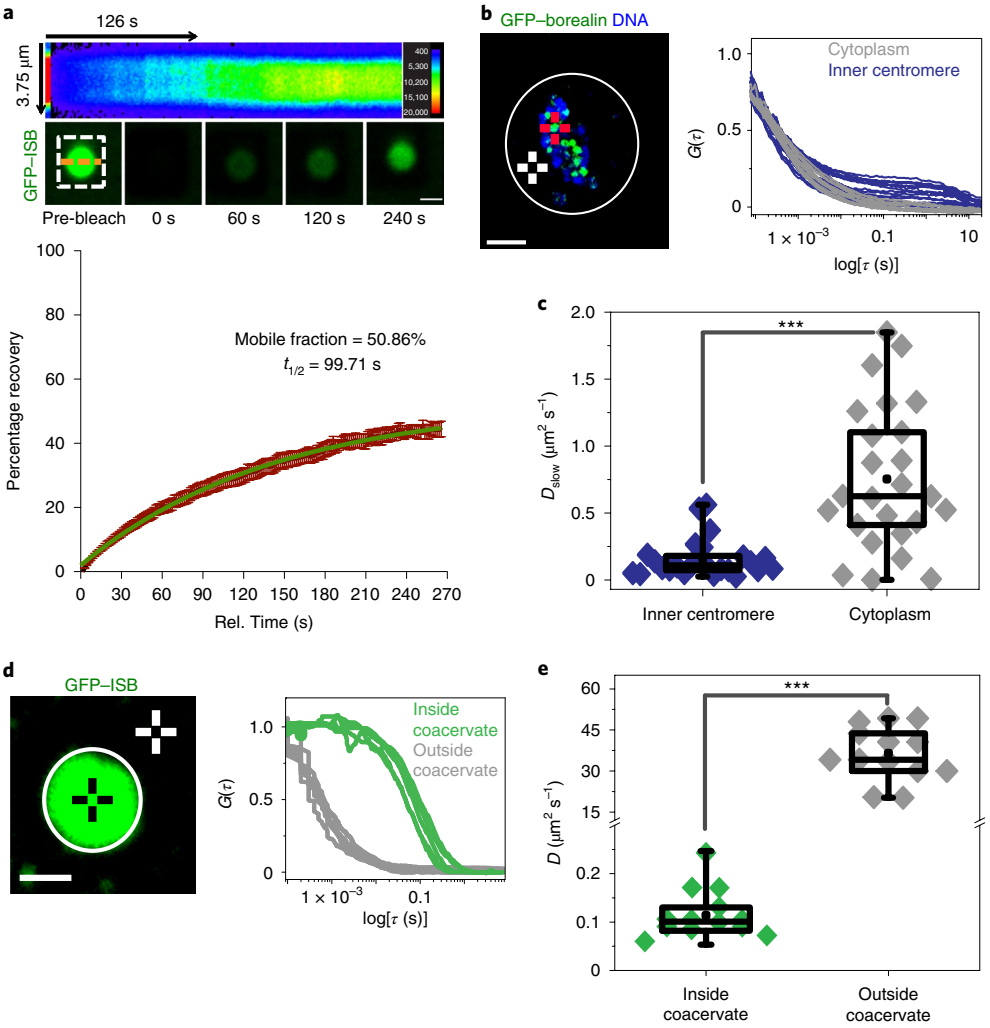

Fig. 2 | The dynamics of the CPC subunits in coacervates are similar to those measured in the inner centromere. a, FRAP analysis of GFP–ISB coacervates. GFP–INCENP$^{1–58}$ was photobleached in the ISB coacervates and fluorescence recovery was monitored; the white dotted box indicates the bleached area. Top, pseudo-coloured kymograph of the fluorescence intensity at the orange dotted line of the FRAP experiment. Pseudo-colour in the kymograph corresponds to the fluorescence intensity as indicated by the colour scale in the top right; three independent repeats were performed. Bottom, time-lapse images from the FRAP experiment. Graph of fluorescence recovery after photobleaching inside the droplet over time. Data are mean ± s.e.m. at each time point; $n = 14$ coacervates, combined data from three independent repeats. The green line indicates a curve fitted with one phase-association kinetics equation. The mobile fraction is 50.86% with a 95% confidence interval ranging from 48.89% to 52.82%. $t_{1/2} = 99.71$ s with a 95% confidence interval ranging from 90.13 s to 111.6 s. **b**, Image of a mitotic cell expressing GFP–borealin treated with 3.3 µM nocodazole (left). The red and white crosshairs are examples of the inner-centromeric and cytoplasmic regions selected for FCS measurements, respectively; three independent repeats were performed. Scale bar, 10 µm. Right, normalized autocorrelation function (G(τ)), where τ is the lag time, of GFP–borealin measurements at the inner centromere (blue) or in the cytoplasm (grey). **c**, Box and whisker plot of the diffusion rate of GFP–borealin as part of CPC (D_{slow}) measured at the inner centromere ($n = 25$ inner centromeres) or the cytoplasm ($n = 25$ spots in cytoplasm) calculated from the graph shown in **b**; combined data from three independent repeats; $P = 3.34 \times 10^{-6}$. **d**, Image of GFP–ISB coacervate. The black and white crosshairs are examples of regions selected for FCS measurements inside coacervates or outside coacervates, respectively (left; three independent repeats). Scale bar, 1 µm. Right, normalized autocorrelation function (G(τ)) of GFP–ISB measurements inside the coacervates (green) or outside the coacervates (grey). **e**, Box and whisker plot of GFP–ISB diffusion rate inside the coacervates ($n = 13$ coacervates) or outside the coacervates ($n = 14$ spots outside coacervates); combined data from three independent repeats. Statistical analysis was performed using two-tailed *t*-tests; $P = 1.54 \times 10^{-8}$. Unless otherwise indicated, ***$P < 0.001$; **$P < 0.01$; *$P < 0.05$; ns, $P > 0.05$. For box and whisker plots, data are median (line), 25–75th percentiles (box) and 5–95th percentiles (whiskers). Source data for **a**–**e** are provided in Supplementary Table 2.

inhibited phase separation (increasing the saturation concentration to ~9 µM; Fig. 4d). By contrast, neither GFP nor SGO1$^{1–112}$ affected the saturation concentration of ISB (Fig. 4d).

Borealin is phosphorylated at multiple sites by CDK1 during mitosis to promote inner-centromere localization. We measured the saturation concentration of ISB after phosphorylation by Cyclin-B-CDK1. Pre-incubation of ISB with Cyclin-B-CDK1 and ATP reduced the saturation concentration from 10 µM to ~8 µM (Fig. 4e). This effect was not observed in the absence of ATP (Fig. 4e). The effect of CDK1 phosphorylation is probably an underestimate as it is unlikely that the ISB was fully phosphorylated in vitro. These in vitro data strongly support a model in which the initial local concentration of the CPC on chromatin due to the phosphorylated-histone marks induces phase separation at the inner centromere and

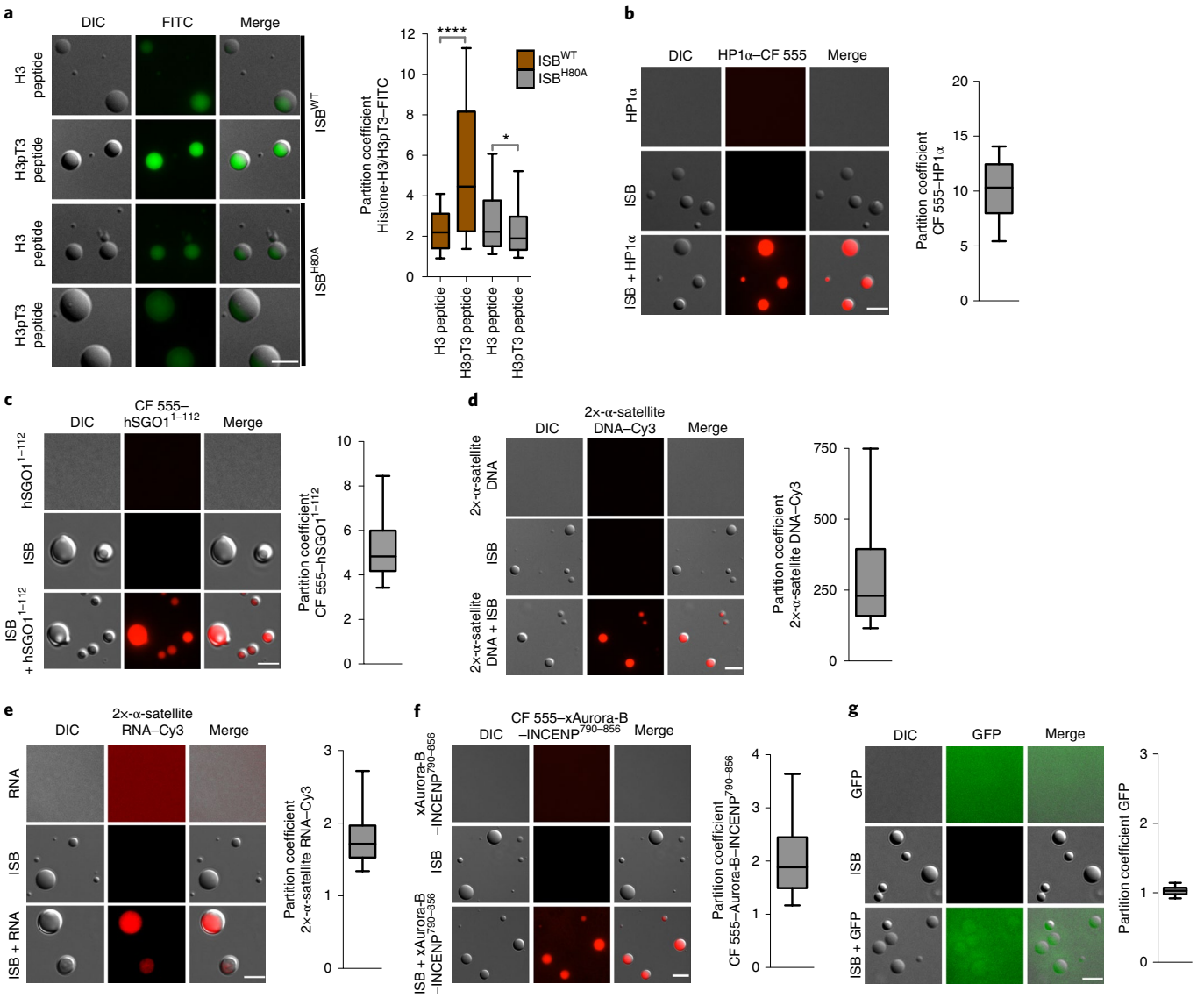

Fig. 3 | Components of the inner centromere are enriched in ISB coacervates. a–g ISB coacervates were mixed with the indicated fluorescent inner-centromere constituents and imaged for enrichment. **a**, Representative micrographs showing enrichment of FITC–histone H3 peptide or FITC–histone H3pT3 peptide in ISB^{WT} or ISB^{H80A} mutant coacervates. Control micrographs for FITC peptide alone and ISB-WT or ISB-H80A mutant coacervates alone are shown in Supplementary Fig. 4d. The graph shows the partition coefficient of the H3 and H3pT3 peptides in ISB^{WT} or ISB^{H80A} mutant coacervates (82, 63, 76 and 95 coacervates were analysed for ISB^{WT} and H3, ISB^{WT} and H3pT3, ISB^{H80A} and H3, and ISB^{H80A} and H3pT3, respectively). Statistical analysis was performed using two-tailed Mann–Whitney *U*-tests. $^{****}P < 0.0001$; $^{*}P = 0.0498$. **b**, Purified HP1 protein was labelled with CF555 (CF555–HP1α), incubated with ISB coacervates and imaged. Representative micrograph and graph of partition coefficient ($n = 171$ coacervates). **c–g**, The partition coefficient of CF555–hSGO1$^{1–112}$ (**c**; $n = 129$ coacervates), 2×-α-satellite DNA–Cy3 (**d**; n = 193 coacervates), 2×-α-satellite RNA–Cy3 (**e**; $n = 129$ coacervates), CF555–xAurora-B–INCENP$^{790–856}$ (**f**; $n = 200$ coacervates) and GFP (**g**; $n = 133$ coacervates) was measured as in **b** in the ISB phase. For **a–g**, data are combined from three independent experiments. Scale bars, 5 µm. For box and whisker plots, data are median (line), 25–75th percentiles (box) and 5–95th percentiles (whiskers). Source data for **c–g** are provided in Supplementary Table 2.

then other factors, such as the presence of pHP1α and CDK1 activity, further enhance phase separation of the CPC.

Borealin undergoes phase separation in vivo. We used the Cry2 optoDroplet system to test whether borealin can undergo phase separation in vivo[37]. A phase-separating protein fused to the light-inducible dimerizing protein Cry2 will form droplets/punctae in vivo after exposure to blue light. We fused Cry2 to the borealin subunit because borealin had the highest likelihood to participate in phase separation among CPC subunits according to a prediction by CatGranule, which is a machine-learning algorithm that predicts the propensity of a protein to undergo phase separation (Supplementary Fig. 5g). Around 95% of cells expressing mCherry–Cry2–borealin formed distinct punctae in interphase nuclei after exposure to blue light (Fig. 5a, Supplementary Fig. 5a). By contrast, none of the cells expressing mCherry–Cry2 formed foci (Fig. 5a).

Ectopic targeting of phase-separating low-complexity protein regions to a specific genomic locus has been shown to induce foci in interphase cells that can be identified by differential interference contrast (DIC) imaging[38]. Borealin fused to mCherry–LacI was targeted to a locus on chromosome 1 that contained 200 copies of 256×LacO/96×tetracycline-responsive element (TRE) arrays.

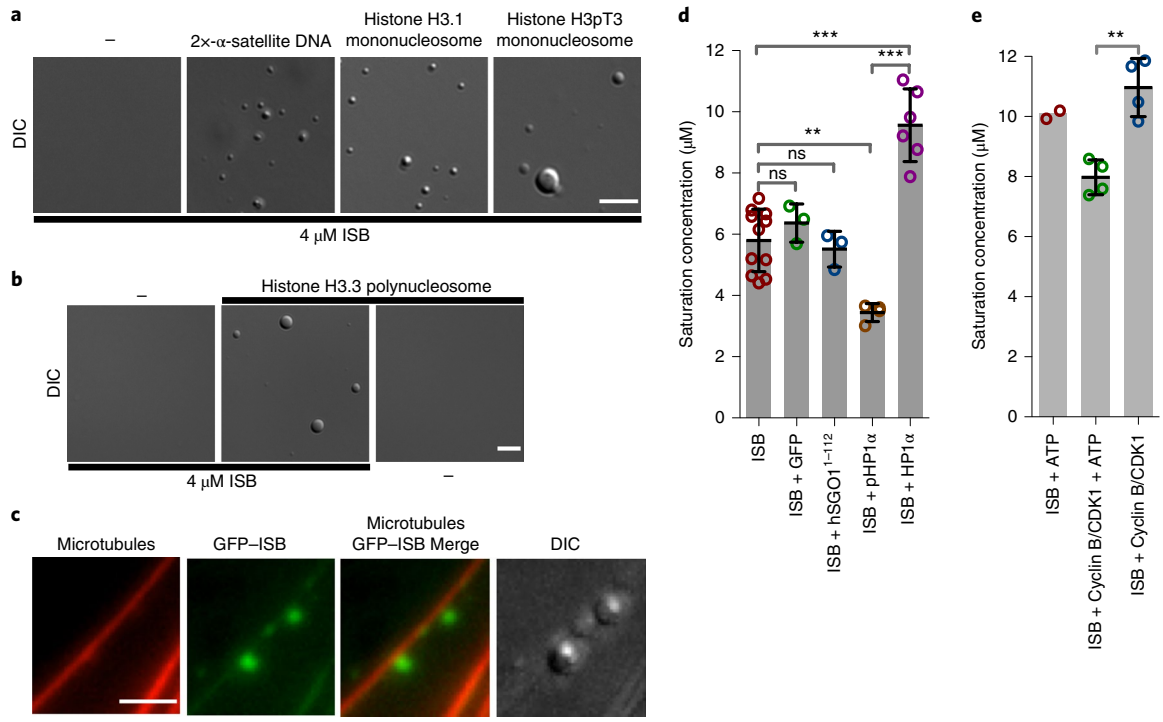

Fig. 4 | Inner-centromere components can induce ISB phase separation. a, Micrographs showing phase separation of 4 μM ISB^{WT} induced by 13 ng μl^{-1} of 2x-α-satellite, histone H3.1 or H3pT3 mononucleosomes in buffer containing 150 mM NaCl. Scale bar, 5 μm. **b**, Micrographs showing phase separation of 4 μM ISB^{WT} induced by 80 ng μl^{-1} histone H3.3 polynucleosomes in buffer containing 150 mM NaCl. Scale bar, 5 μm. **c**, Micrographs showing phase separation of GFP–ISB (5 μM) induced on paclitaxel-stabilized rhodamine-labelled microtubules (1 μM) in buffer containing 150 mM NaCl. Scale bar, 3 μm. For **a**–**c** the experiments were repeated independently three times. **d**, Mitotically phosphorylated HP1α lowers the saturation concentration of ISB. Saturation concentrations of ISB alone ($n=11$) or ISB mixed with equimolar amounts of GFP ($n=3$), hSGO1$^{1–112}$ ($n=3$), pHP1α ($n=3$) and HP1α ($n=6$) in buffer containing 150 mM NaCl measured using a spin-down method. **e**, CDK1 phosphorylation lowers the saturation concentration of ISB. Saturation concentration of ISB after incubation with ATP ($n=2$), Cyclin-B/CDK1 and ATP ($n=4$), or Cyclin-B/CDK1 ($n=4$) in kinase buffer containing 150 mM NaCl measured using a spin-down method. For **d** and **e**, *n* is the number of independent experiments; statistical analyses were performed using one-way analysis of variance (ANOVA) followed by Bonferroni's multiple comparison test. Data are mean ± s.d.; circles show the individual data points. Source data for **d** and **e** are provided in Supplementary Table 2.

The targeting of borealin generated a distinct DIC focus compared with chromatin next to it (Fig. 5b, Supplementary Fig. 5b). Targeting mCherry–LacI did not generate DIC foci (Fig. 5b, Supplementary Fig. 5b). The change in DIC signal was difficult to distinguish on highly condensed mitotic chromosomes, restricting our analysis to interphase nuclei. We conclude that borealin/CPC can undergo phase separation in vivo either on artificial targeting to a chromosomal locus or on increase in valency.

The CPC displays condensate-like properties at the inner centromere. Inhibiting weak hydrophobic interactions by using the aliphatic alcohol 1,6-hexanediol disrupts many phase-separated organelles in cells[39]. 1,6-hexanediol treatment reduced the enrichment of CPC in the inner centromere and the level of CPC redistributed to the chromosome arms (Fig. 5c,d). 1,6-hexanediol also disrupted ISB coacervates in vitro (Supplementary Fig. 5c).

Our in vitro analysis suggested that the CPC at inner centromeres should be sensitive to increases in ionic strength. Treatment with the cell-permeable salt ammonium acetate has previously been used to disrupt the phase separation and gelation of repeat-containing RNA in cells[40] and it has also been shown to disrupt ISB coacervates in vitro (Supplementary Fig. 5d). Ammonium acetate treatment for 2 min displaced the CPC from the inner centromeres of mitotic cells (Fig. 5e,f). Inner-centromeric Aurora-B completely recovered 2 min after ammonium acetate washout (Fig. 5e,f).

PEG-3350 substantially reduces the saturation concentration of ISB, allowing phase separation to occur in the presence of high NaCl concentrations (Fig. 1b–d, Supplementary Fig. 5e) and providing an opportunity to investigate whether the reduction in CPC levels was due to disruption of phase separation or other effects of increasing ionic concentrations. High levels of salt significantly reduced the levels of endogenously tagged Aurora-B and INCENP at inner centromeres of isolated mitotic chromosomes. By contrast, the CPC was maintained at high levels in the presence of high levels of salt and PEG-3350 (Fig. 5g,h, Supplementary Fig. 5f). Thus, treatments that disrupt membraneless organelles disrupt the CPC at inner centromeres.

Borealin-dependent phase separation drives inner-centromere localization of the CPC. We identified mutants of borealin that are defective in phase separation. We deleted two regions in the central unstructured region of borealin that were predicted to have a high propensity to undergo phase separation by CatGranule[41,42] (Fig. 6a, Supplementary Fig. 5g–i). ISB lacking amino acids 139–160 of borealin was deficient in both spontaneous and DNA-induced phase separation (Fig. 6b–d). By contrast, ISB$^{Δ165–180}$ behaves similar to wild-type ISB (ISB^{WT}) in these assays (Fig. 6b–d). These deletions did not compromise ISB complex formation or hydrodynamic properties (Supplementary Fig. 1a,b). Borealin$^{Δ139–160}$ was also deficient in the optoDroplet assay (Fig. 5a, Supplementary Fig. 5a). The deleted region in borealin$^{Δ139–160}$ is adjacent to a CDK phosphorylation region that has been postulated to interact with SGO1. We did not change any CDK phosphorylation sites in any of our mutants, but we still checked whether the interaction between

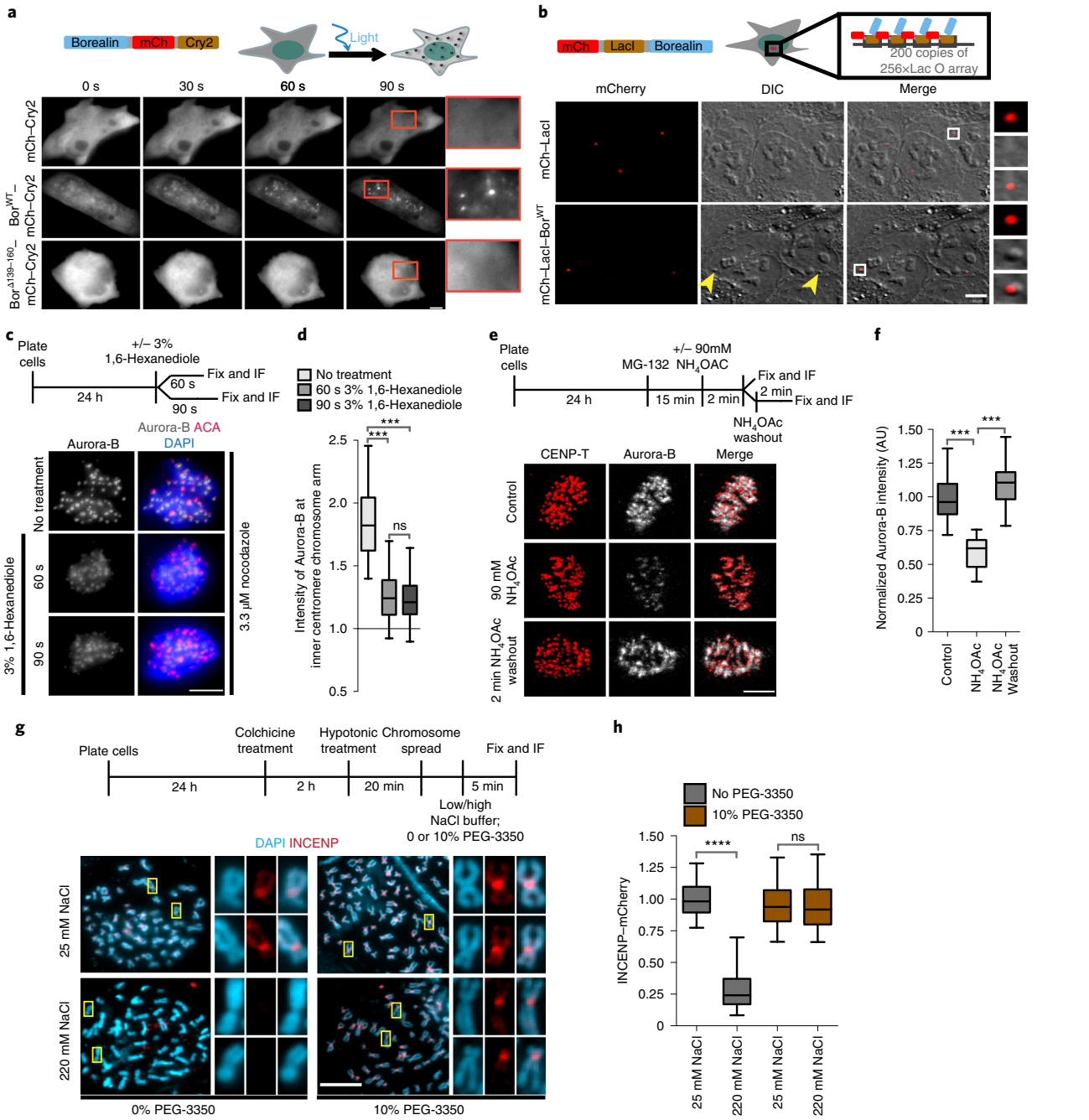

Fig. 5 | Borealin undergoes phase separation in vivo and inner-centromeric CPC is sensitive to inhibitors of phase separation. a, An optoDroplet assay. Cells expressing mCherry–Cry2–borealin were exposed to blue light followed by time-lapse imaging. Quantification is provided in Supplementary Fig. 5a. Bor, borealin; mCh, mCherry . **b**, Schematic of a system to target LacI–borealin to a LacO array (top). Bottom, DIC and mCherry images of cells expressing mCherry–LacI or mCherry–LacI–borealin^{WT}, showing the formation of DIC spots (yellow arrowheads) at the LacO array after targeting. The white boxes indicate the regions magnified on the right. Quantification is provided in Supplementary Fig. 5b. **c**,**d**, The experimental setup for **c** and **d** (**c**, top). IF, immunofluorescence analysis. Images (**c**, bottom) and quantification (**d**) of cells arrested in mitosis using 3.3 μM nocodazole and treated with vehicle control for 90 s or 3% 1,6-hexanediol for 60 s or 90 s, and stained for Aurora-B (grey), ACA (red) and DAPI (blue); $n = 158$ from 11 cells, $n = 149$ from 10 cells and $n = 190$ from 12 cells for no treatment, 60 s and 90 s 1,6-hexanediol treatment, respectively. **e**, The experimental setup for **e** and **f** (top). Bottom, images showing Aurora-B (grey) and CENP-T (red) in cells treated with vehicle control or 90 mM NH_4OAc or 2 min after NH_4OAc washout. **f**, Aurora-B-fluorescence intensity was normalized to the control under the conditions indicated in **e**; $n = 131$ from 11 cells for control and $n = 76$ from 9 cells each for NH_4OAC treatment and washout. For **d** and **f**, statistical analysis was performed using one-way ANOVA followed by Dunn's multiple comparison test. **g**, The experimental setup for **g** and **h** (top). Bottom, chromosome spread showing DAPI (blue) and INCENP–mCherry (red) under the indicated conditions. The yellow boxes indicate the regions magnified on the right. **h**, Intensity of INCENP–mCherry normalized to its intensity at the inner centromeres under no PEG-3350 and 25 mM NaCl condition; the graph of experiment shown in **g**; $n = 318$, 430, 412 and 892 for 25 mM NaCl, 220 mM NaCl, 25 mM NaCl and 10% PEG-3350, and 220 mM and 10% PEG-3350, respectively. Statistical analysis was performed using two-tailed *t*-tests; ns, $P = 0.6688$. *n* is the number of inner centromeres measured. For **a**, **c**, **g** and **e**, scale bars, 5 μm; for **b**, scale bar, 7 μm. For **a**–**h**, two independent experimental repeats were performed. For box and whisker plots, data are median (line), 25–75th percentiles (box) and 5–95th percentiles (whiskers). Source data for **d**, **f** and **h** are provided in Supplementary Table 2.

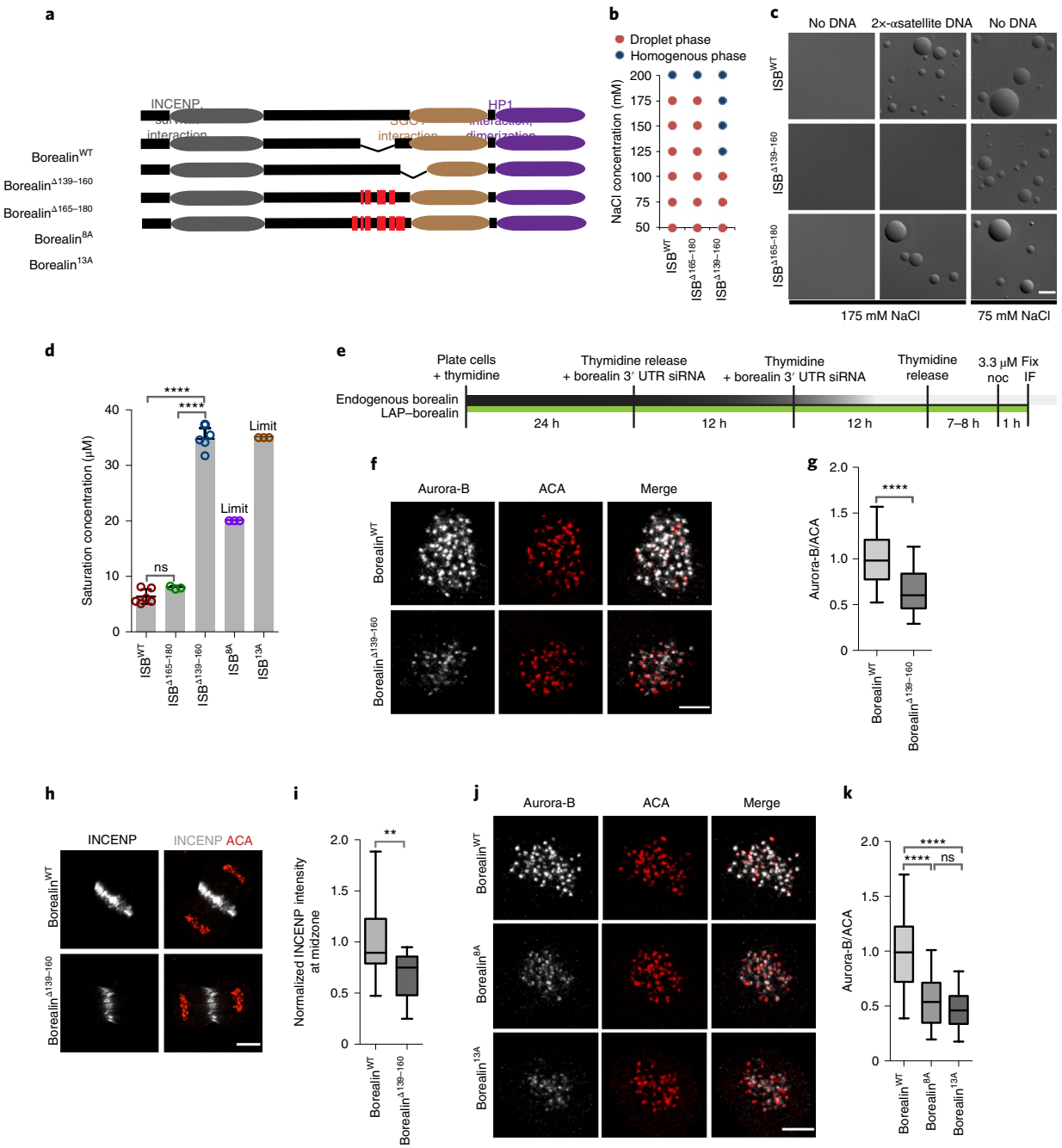

Fig. 6 | The phase-separation property of the CPC is crucial for its localization to inner centromeres and spindle midzones. a, A schematic of borealin domains and mutants tested in **b**–**k**. The red vertical lines indicate the mutated residues. **b**, Phase of 20 μM ISB^{WT}, ISB$^{Δ165–180}$ or ISB$^{Δ139–160}$ at the indicated NaCl concentration. **c**, Micrographs of ISB^{WT} or mutant at the indicated condition in the presence of 8 μM ISB and with or without 58 ng μl^{-1} 2×-α-satellite DNA; the experiment was repeated twice. **d**, Saturation concentration of ISB^{WT} ($n=6$), ISB$^{Δ165–180}$ ($n=3$), ISB$^{Δ139–160}$ ($n=5$), ISB^{8A} ($n=3$) and ISB^{13A} ($n=3$) in buffer containing 150 mM NaCl. *n* is the number of independent experiments. 'Limit' indicates that phase separation was not observed at the maximum concentration that could be tested. Data are mean ± s.d.; circles show individual data points. Statistical analysis was performed using one-way ANOVA followed by Bonferroni's multiple comparison test. **e**, Experimental design for knockdown and replacement of endogenous borealin for **f**, **g**, **j** and **k**. Noc, nocodazole. **f**, Aurora-B and ACA in cells rescued with either LAP-borealin^{WT} or LAP-borealin$^{Δ139–160}$ and treated with 3.3 μM nocodazole. **g**, Normalized intensity of Aurora-B and ACA from the experiment shown in **f**; $n=235$ from 13 cells for LAP-borealin^{WT}, $n=195$ from 14 cells for LAP-borealin$^{Δ139–160}$. Statistical analysis was performed using a two-tailed unpaired *t*-test with Welch's correction. **h**, Staining of INCENP and ACA in anaphase cells rescued with either LAP-borealin^{WT} or LAP-borealin$^{Δ139–160}$. **i**, INCENP intensity normalized to the mean intensity of LAP-borealin^{WT} at the spindle midzone from the experiment shown in **h** ($n=16$ and $n=15$ spindle midzones for LAP-borealin^{WT} and LAP-borealin$^{Δ139–160}$, respectively). Statistical analysis was performed using a two-tailed *t*-test. $^{**}P=0.0045$. **j**, Aurora-B and ACA in cells rescued with LAP-borealin^{WT} ($n=154$ from 9 cells), LAP-borealin^{8A} ($n=123$ from 8 cells) or LAP-borealin^{13A} ($n=97$ from 9 cells) and treated with 3.3 μM nocodazole. **k**, Normalized intensity of Aurora-B and ACA from the experiment shown in **j**. *n* indicates the number of inner centromeres measured for **g** and **k**. For **f**–**k**, two independent repeats were performed. Statistical analysis was performed using one-way ANOVA followed by Bonferroni's multiple comparison test. For **c**, **f**, **h** and **j**, scale bars, 5 μm. For box and whisker plots, data are median (line), 25–75th percentiles (box) and 5–95th percentiles (whiskers). Source data for **b**, **d**, **g**, **i** and **k** are provided in Supplementary Table 2.

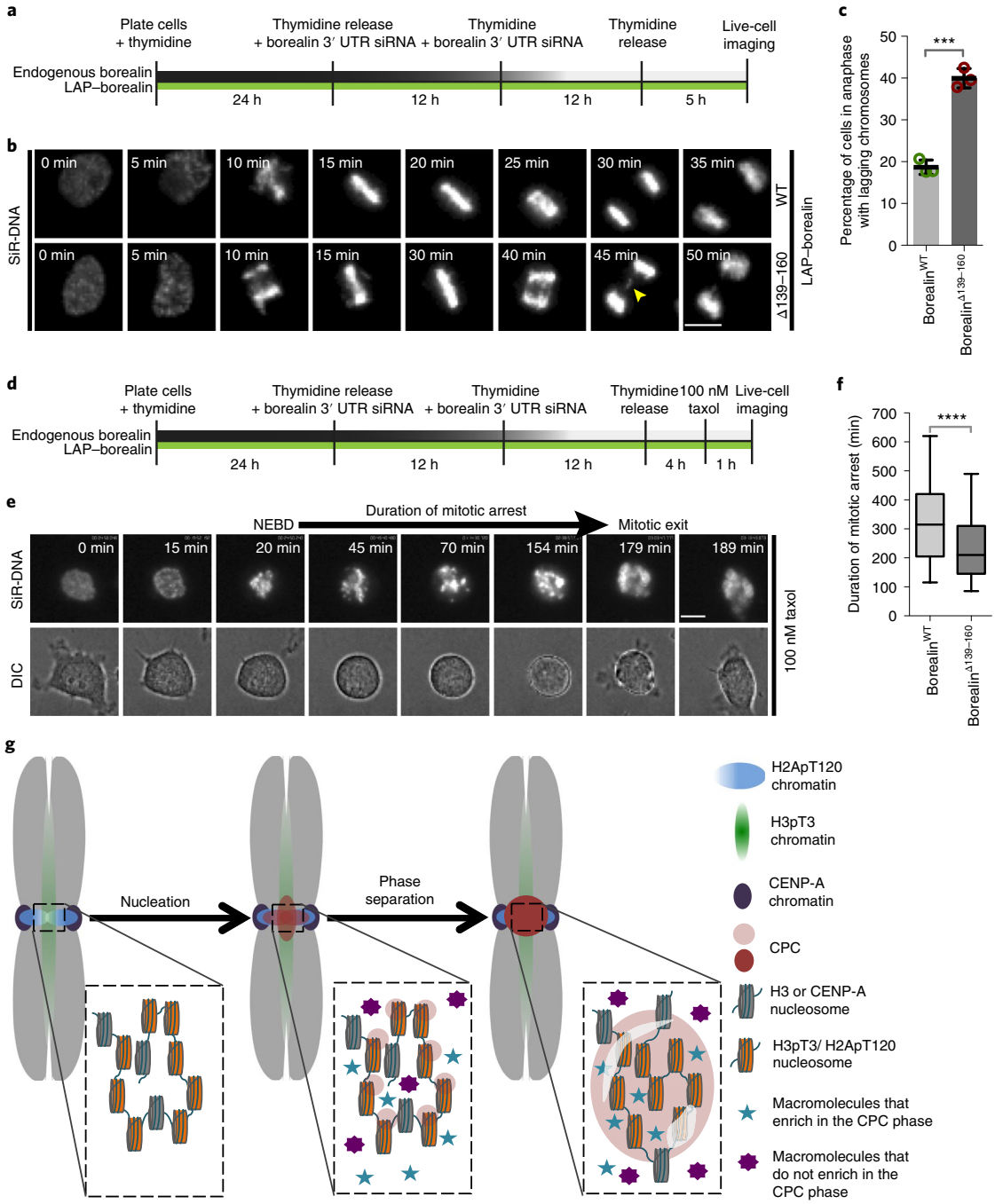

Fig. 7 | The phase-separation property of the CPC is important for its mitotic functions. a, Schematic of the experimental setup for **b** that was used to analyse mitotic progression during the first mitosis after depletion of endogenous borealin in cells complemented with either LAP–borealin^{WT} or LAP–borealin$^{\Delta139-160}$. **b**, Representative frames from the time-lapse images of cells complemented with either LAP–borealin^{WT} or LAP–borealin$^{\Delta139-160}$ undergoing mitosis. The yellow arrow indicates the lagging chromosomes in anaphase. Three independent repeats were performed. **c**, Graph showing the percentage of anaphases with lagging chromosomes in cells rescued with LAP–borealin^{WT} or LAP–borealin$^{\Delta139-160}$. Data are mean ± s.d. from $n = 3$ independent experiments; 121, 107 and 125 cells were analysed for LAP–borealin^{WT}; 106, 103 and 86 cells were analysed for LAP–borealin$^{\Delta139-160}$; circles show individual data points. Statistical analysis was performed using two-tailed unpaired *t*-tests. ***$P = 0.0002$. A cumulative-frequency graph of the duration of taxol arrest and of various phases of mitosis is provided in Supplementary Fig. 7. **d**, Schematic of the experimental setup for **e** that was used to analyse the duration of taxol-induced mitotic arrest in first mitosis after replacement of endogenous borealin with either LAP–borealin^{WT} or LAP–borealin$^{\Delta139-160}$. **e**, Representative frames from the time-lapse images of cells undergoing mitosis in the presence of 100 nM paclitaxel. NEBD, time of nuclear envelope breakdown. The duration from the time of nuclear envelope breakdown to mitotic exit or cell death is defined as the duration of mitotic arrest. Two independent repeats were performed. **f**, Graph showing the duration of mitotic arrest in cells that were rescued with LAP–borealin^{WT} or LAP–borealin$^{\Delta139-160}$; $n = 220$ cells were analysed per condition; combined data from two independent experiments are shown. For box and whisker plots, data are median (line), 25–75th percentiles (box) and 5–95th percentiles (whiskers). Statistical analysis was performed using a two-tailed Mann–Whitney *U*-test. For **b** and **e**, SiR-DNA was used to visualize DNA. Scale bars, 5 µm. **g**, A model for the localization of the CPC to the inner centromere driven by initial nucleation by phosphorylated-histone marks followed by phase separation of the CPC. Furthermore, some components are enriched in the CPC coacervates (blue stars), whereas others are excluded (purple eight-pointed star). Source data for **c** and **f** are provided in Supplementary Table 2.

ISB and SGO1 was affected by the deletion. ISB^{WT} and ISB$^{\Delta 139-160}$ interacted equally well with hSGO1$^{1-112}$ inside droplets formed in 10% PEG-3350, which lowers the saturation concentration of ISB and enables the formation of coacervates even with the ISB$^{\Delta 139-160}$ protein (Supplementary Fig. 6l,m). CDK phosphorylation was not essential for the interaction between ISB^{WT} and SGO1$^{1-112}$ within coacervates (Fig. 3c), rather, we found that CDK phosphorylation lowered the saturation concentration of ISB (Fig. 4e), suggesting an alternative explanation to the requirement of CDK in inner-centromere formation. We cannot completely rule out the possibility that the region that drives phase separation also has an unappreciated second function that controls CPC localization.

The strong regulation of ISB phase separation by ionic concentration in vivo and in vitro suggested that charge is important for phase separation. We mutated eight positively charged residues in the region of amino acids 139–160 of borealin to alanine (ISB^{8A}). We also mutated five additional positively charged residues surrounding the region of amino acids 139–160 to alanine (ISB^{13A}; Fig. 6a, Supplementary Fig. 5g). Both of these mutants were defective in phase separation (Fig. 6d).

To study the effect of these mutations on the localization of the CPC during mitosis, we depleted the endogenous borealin using short interfering RNA (siRNA) and complemented the cells with either LAP-tagged (GFP and S-peptide) borealin^{WT} or borealin lacking the amino acids 139–160 (borealin$^{\Delta 139-160}$; Supplementary Fig. 6a,c). The borealin$^{\Delta 139-160}$ mutant had reduced levels of CPC in the inner centromere and spindle midzones compared with the WT (Fig. 6e–i, Supplementary Fig. 6d). H3T3ph, H2AT120ph and hSGO1 levels at the inner centromere were similar in cells complemented with borealin^{WT} and borealin$^{\Delta 139-160}$ (Supplementary Fig. 6f–k). Cells complemented with borealin^{8A} or borealin^{13A} also had lower levels of Aurora-B in the inner centromere (Fig. 6j,k, Supplementary Fig. 6b). We conclude that the CPC exists in a phase-separated state at the inner centromere.

The phase-separation property of the CPC is important for its mitotic function. We depleted endogenous borealin in cells and complemented them with either borealin^{WT} or borealin$^{\Delta 139-160}$ and imaged the cells going through mitosis. Cells expressing borealin$^{\Delta 139-160}$ were deficient in correcting improper kinetochore–microtubule attachments compared with cells expressing borealin^{WT}, as measured by the frequency of anaphases with lagging chromosomes (Fig. 7a–c). A modest increase in the duration of mitosis was observed in cells expressing borealin$^{\Delta 139-160}$ (Supplementary Fig. 7a–c). Furthermore, paclitaxel-induced spindle-assembly checkpoint arrest was deficient in cells expressing borealin$^{\Delta 139-160}$ compared with cells expressing borealin^{WT} (Fig. 7d–f, Supplementary Fig. 7d). We conclude that the phase-separation property of the CPC is important for correcting kinetochore–microtubule attachments and maintaining the spindle checkpoint.

Discussion

We demonstrate that phase separation is a central biochemical function of the CPC that works in concert with Aurora-B kinase activity to regulate chromosome segregation. The centromere-targeting region of the CPC undergoes phase separation driven by an unstructured region on borealin that is critical for the mitotic functions of the CPC. Phase-separated CPC retained its ability to interact with many inner-centromere components and some stimulated coacervate formation. We were able to provide six lines of evidence that the CPC exists in a phase-separated state at the inner centromeres. First, the CPC centromere-targeting subunits form coacervates at concentrations below those measured at the inner centromere. Second, the turnover and diffusion rates of the CPC subunits in coacervates and in the inner centromere are strongly correlated. Third, 1,6-hexanediol or ammonium acetate, which disrupt phase separation, reduced inner-centromeric CPC. Fourth, ectopic targeting of the borealin subunit to a LacO array imparted droplet-like optical properties to this chromatin region. Fifth, borealin subunits formed foci in the optoDroplet assay. Sixth, borealin mutants that reduced the ability of the CPC to undergo phase separation in vitro were deficient in localizing to inner centromeres and spindle midzones and at regulating mitotic events. Thus, we suggest that phase separation underlies the unique properties of the inner centromere and it may become more appropriate to refer to this chromosome area as the inner-centromere body to reflect this insight.

Although ISB can undergo phase separation on its own in vitro, the fact that nucleosomes, HP1α and CDK phosphorylation all lowered the saturation concentration suggests that they form a multivalent interaction network that drives the formation of the inner centromere body. This multivalent interaction network may also explain how interactions that are either sub-stoichiometric (SGO1) or more dynamic (survivin) can still anchor CPC stably at the inner centromere.

CPC signals from inner centromeres are chromosome autonomous[1]. Phase separation may provide a mechanism to restrict signalling events to a single chromosome, although we do not think that kinase activity can be absolutely contained as it must escape droplets to generate gradients of soluble activity on chromatin and from the centre of the anaphase spindle[10,11]. The CPC distinguishes merotelic from amphitelic attachments by interaction with microtubules that lie near inner-centromeric chromatin[43]. The propensity of the CPC to undergo phase separation on either chromatin or microtubules suggests the exciting possibility that merotelic K-fibre bundles act as conduits for phase-separated CPC to flow from the inner centromeres onto merotelic microtubules as a mechanism to correct attachments.

Biomolecular condensates provide a mechanism to concentrate components to control biochemical reactions within cells[4]. We have shown that components of the inner centromere preferentially partition to the ISB condensate, suggesting that functions in the inner centromere, such as cohesion protection, emerge from the concentration of key proteins in coacervates (Fig. 7g). Our in vitro experiments were performed using a subassembly that contains all of the activities required to localize the CPC to inner centromeres; however, we have not been able to purify the full-length CPC and, therefore, it is possible that the rest of the CPC may alter its propensity to form coacervates or interact with other proteins.

Our data suggests that pericentric heterochromatin undergoes a switch from HP1α as the primary liquid-demixing agent in interphase to the CPC during mitosis. HP1α initiates the activation of Aurora-B kinase activity before mitosis[30]. The CPC disrupts HP1α binding to H3K9me3 in mitosis[44,45] and then directly recruits HP1α to the inner centromere[30,31,46]. We have shown that mitotically phosphorylated HP1α[36] increased ISB phase separation, suggesting that the liquid-demixing properties of HP1α and the CPC cooperate to control pericentric heterochromatin.

How cells assemble and disassemble phase-separated bodies is an area of intense research. We suggest that the inner-centromere body is an excellent system to dissect these activities as their assembly and disassembly is spatiotemporally defined. We propose that the initial localization of the CPC through phosphorylated-histone marks (nucleation) concentrates the CPC on mitotic chromatin until it reaches a critical concentration, after which the CPC undergoes phase separation (Fig. 7g).

Online content

Any methods, additional references, Nature Research reporting summaries, source data, statements of code and data availability and associated accession codes are available at https://doi.org/10.1038/s41556-019-0376-4.

Received: 21 June 2018; Accepted: 19 July 2019;
Published online: 3 September 2019

References

1. Trivedi, P. & Stukenberg, P. T. A centromere-signaling network underlies the coordination among mitotic events. *Trends Biochem. Sci.* **41**, 160–174 (2016).
2. Bloom, K. S. Centromeric heterochromatin: the primordial segregation machine. *Annu. Rev. Genet.* **48**, 457–484 (2014).
3. Jaqaman, K. et al. Kinetochore alignment within the metaphase plate is regulated by centromere stiffness and microtubule depolymerases. *J. Cell Biol.* **188**, 665–679 (2010).
4. Banani, S. F., Lee, H. O., Hyman, A. A. & Rosen, M. K. Biomolecular condensates: organizers of cellular biochemistry. *Nat. Rev. Mol. Cell Biol.* **18**, 285–298 (2017).
5. Larson, A. G. et al. Liquid droplet formation by HP1α suggests a role for phase separation in heterochromatin. *Nature* **547**, 236–240 (2017).
6. Strom, A. R. et al. Phase separation drives heterochromatin domain formation. *Nature* **547**, 241–245 (2017).
7. Sabari, B. R. et al. Coactivator condensation at super-enhancers links phase separation and gene control. *Science* **361**, eaar3958 (2018).
8. Mahen, R. et al. Comparative assessment of fluorescent transgene methods for quantitative imaging in human cells. *Mol. Biol. Cell* **25**, 3610–3618 (2014).
9. Sessa, F. et al. Mechanism of aurora B activation by INCENP and inhibition by hesperadin. *Mol. Cell* **18**, 379–391 (2005).
10. Fuller, B. G. et al. Midzone activation of aurora B in anaphase produces an intracellular phosphorylation gradient. *Nature* **453**, 1132–1136 (2008).
11. Wang, E., Ballister, E. R. & Lampson, M. A. Aurora B dynamics at centromeres create a diffusion-based phosphorylation gradient. *J. Cell Biol.* **194**, 539–549 (2011).
12. Yamagishi, Y., Honda, T., Tanno, Y. & Watanabe, Y. Two histone marks establish the inner centromere and chromosome bi-orientation. *Science* **330**, 239–243 (2010).
13. Wang, F. et al. Histone H3 Thr-3 phosphorylation by haspin positions aurora B at centromeres in mitosis. *Science* **330**, 231–235 (2010).
14. Kelly, A. E. et al. Survivin reads phosphorylated histone H3 threonine 3 to activate the mitotic kinase aurora B. *Science* **330**, 235–239 (2010).
15. YamagishiY., HondaT., TannoY. & WatanabeY. Two histone marks establish the inner centromere and chromosome bi-orientation. *Science* **330**, 239–243 (2010).
16. Tsukahara, T., Tanno, Y. & Watanabe, Y. Phosphorylation of the CPC by Cdk1 promotes chromosome bi-orientation. *Nature* **467**, 719–723 (2010).
17. Niedzialkowska, E. et al. Molecular basis for phosphospecific recognition of histone H3 tails by survivin paralogues at inner centromeres. *Mol. Biol. Cell* **23**, 1457–1466 (2012).
18. Du, J., Kelly, A. E., Funabiki, H. & Patel, D. J. Structural basis for recognition of H3T3ph and Smac/DIABLO N-terminal peptides by human survivin. *Structure* **20**, 185–195 (2012).
19. Delacour-Larose, M., Molla, A., Skoufias, D. A., Margolis, R. L. & Dimitrov, S. Distinct dynamics of aurora b and survivin during mitosis. *Cell Cycle* **3**, 1418–1426 (2004).
20. Beardmore, V. A. Survivin dynamics increases at centromeres during G2/M phase transition and is regulated by microtubule-attachment and aurora B kinase activity. *J. Cell Sci.* **117**, 4033–4042 (2004).
21. Wühr, M. et al. Deep proteomics of the *Xenopus laevis* egg using an mRNA-derived reference database. *Curr. Biol.* **24**, 1467–1475 (2014).
22. Hindriksen, S., Lens, S. M. A. & Hadders, M. A. The ins and outs of aurora B inner centromere localization. *Front. Cell Dev. Biol.* **5**, 112 (2017).
23. Hauf, S. et al. The small molecule Hesperadin reveals a role for aurora B in correcting kinetochore-microtubule attachment and in maintaining the spindle assembly checkpoint. *J. Cell Biol.* **161**, 281–294 (2003).
24. Hengeveld, R. C. C., Vromans, M. J. M., Vleugel, M., Hadders, M. A. & Lens, S. M. A. Inner centromere localization of the CPC maintains centromere cohesion and allows mitotic checkpoint silencing. *Nat. Commun.* **8**, 15542 (2017).
25. Klein, U. R., Nigg, E. A. & Gruneberg, U. Centromere targeting of the chromosomal passenger complex requires a ternary subcomplex of borealin, survivin, and the N-terminal domain of INCENP. *Mol. Biol. Cell* **17**, 2547–2558 (2006).
26. Woodruff, J. B. et al. The centrosome is a selective condensate that nucleates microtubules by concentrating tubulin. *Cell* **169**, 1066–1077 (2017).
27. Wheelock, M. S., Wynne, D. J., Tseng, B. S. & Funabiki, H. Dual recognition of chromatin and microtubules by INCENP is important for mitotic progression. *J. Cell Biol.* **216**, 925–941 (2017).
28. Hanley, M. L., Yoo, T. Y., Sonnett, M., Needleman, D. J. & Mitchison, T. J. Chromosomal passenger complex hydrodynamics suggests chaperoning of the inactive state by nucleoplasmin/nucleophosmin. *Mol. Biol. Cell* **28**, 1444–1456 (2017).
29. Wachsmuth, M. et al. High-throughput fluorescence correlation spectroscopy enables analysis of proteome dynamics in living cells. *Nat. Biotechnol.* **33**, 384–389 (2015).
30. Ruppert, J. G. et al. HP1α targets the chromosomal passenger complex for activation at heterochromatin before mitotic entry. *EMBO J.* **37**, e97677 (2018).
31. Liu, X. et al. Chromatin protein HP1α interacts with the mitotic regulator borealin protein and specifies the centromere localization of the chromosomal passenger complex. *J. Biol. Chem.* **289**, 20638–20649 (2014).
32. Abe, Y. et al. HP1-assisted aurora B kinase activity prevents chromosome segregation errors. *Dev. Cell* **36**, 487–497 (2016).
33. Chen, J. et al. Survivin enhances aurora-B kinase activity and localizes aurora-B in human cells. *J. Biol. Chem.* **278**, 486–490 (2003).
34. Wheatley, S. P., Carvalho, A., Vagnarelli, P. & Earnshaw, W. C. INCENP is required for proper targeting of survivin to the centromeres and the anaphase spindle during mitosis. *Curr. Biol.* **11**, 886–890 (2001).
35. Sampath, S. C. et al. The chromosomal passenger complex is required for chromatin-induced microtubule stabilization and spindle assembly. *Cell* **118**, 187–202 (2004).
36. Chakraborty, A., Prasanth, K. V. & Prasanth, S. G. Dynamic phosphorylation of HP1α regulates mitotic progression in human cells. *Nat. Commun.* **5**, 3445 (2014).
37. Shin, Y. et al. Spatiotemporal control of intracellular phase transitions using light-activated optoDroplets. *Cell* **168**, 159–171 (2017).
38. Chong, S. et al. Imaging dynamic and selective low-complexity domain interactions that control gene transcription. *Science* **361**, eaar2555 (2018).
39. Kroschwald, S., Maharana, S. & Simon, A. Hexanediol: a chemical probe to investigate the material properties of membrane-less compartments. *Matters* https://doi.org/10.19185/matters.201702000010 (2017).
40. Jain, A. & Vale, R. D. RNA phase transitions in repeat expansion disorders. *Nature* **546**, 243–247 (2017).
41. Ambadipudi, S., Biernat, J., Riedel, D., Mandelkow, E. & Zweckstetter, M. Liquid–liquid phase separation of the microtubule-binding repeats of the Alzheimer-related protein Tau. *Nat. Commun.* **8**, 275 (2017).
42. Bolognesi, B. et al. A concentration-dependent liquid phase separation can cause toxicity upon increased protein expression. *Cell Rep.* **16**, 222–231 (2016).
43. Trivedi, P. et al. The binding of borealin to microtubules underlies a tension independent kinetochore-microtubule error correction pathway. *Nat. Commun.* **10**, 682 (2019).
44. Hirota, T., Lipp, J. J., Toh, B. H. & Peters, J. M. Histone H3 serine 10 phosphorylation by aurora B causes HP1 dissociation from heterochromatin. *Nature* **438**, 1176–1180 (2005).
45. Fischle, W. et al. Regulation of HP1-chromatin binding by histone H3 methylation and phosphorylation. *Nature* **438**, 1116–1122 (2005).
46. Ainsztein, A. M., Kandels-Lewis, S. E., Mackay, A. M. & Earnshaw, W. C. INCENP centromere and spindle targeting: identification of essential conserved motifs and involvement of heterochromatin protein HP1. *J. Cell Biol.* **143**, 1763–1774 (1998).

Acknowledgements

We thank J. Ellenberg, C. Brangwynne, G. Narlikar and D. Foltz for reagents, and D. Burke and S. Mattada for discussions. P.T.S. and P.T. were funded by NIH grant numbers R01GM124042 and R24OD023697. F.P. and M.A.D. were supported in part by a grant from the NSF (MCB-1615701). M.A.D. and E.G. were funded by NIH grant number P41-GM103540.

Author contributions

P.T. and P.T.S. conceived and designed the study. P.T. performed and analysed all of the experiments, except for those involving FCS, under the guidance of P.T.S. F.P. performed and analysed the FCS experiments under the guidance of M.A.D. and E.G. E.N. provided the human pHP1α and *X. laevis* ISD proteins. P.T. and P.T.S. wrote the manuscript.

Competing interests

The authors declare no competing interests.

Additional information

Supplementary information is available for this paper at https://doi.org/10.1038/s41556-019-0376-4.

Reprints and permissions information is available at www.nature.com/reprints.

Correspondence and requests for materials should be addressed to P.T.S.

Publisher's note: Springer Nature remains neutral with regard to jurisdictional claims in published maps and institutional affiliations.

Methods

Protein purification. BL21(DE3)pLysS cells were transformed with a tricistronic pET28a vector containing sequences for 6×His-INCENP$^{1-58}$, survivin and borealin (WT, Δ139–169 or Δ165–180); for the generation of GFP–ISB, GFP was cloned between 6×His and INCENP$^{1-58}$ to yield a 6×His-GFP-ISB construct. Cells were then grown in the presence of 30 ug ml^{-1} kanamycin to an optical density (OD) of 0.8 and protein expression was induced with 0.45 mM isopropylthiogalactoside (IPTG) for 16–18 h at 18 °C. The medium was also supplemented with 60 mg l^{-1} $ZnCl_2$ and 0.2% glucose. Cells were then pelleted and lysed in buffer containing 500 mM NaCl, 50 mM Tris pH 7.5, 0.5 mM tris(2-carboxyethyl)phosphine (TCEP), 5% glycerol, 5 mM imidazole and protease inhibitor cocktail (Roche) using a EmulsiFlex-C3 homogenizer. The lysate was then cleared by centrifugation and incubated with Ni-NTA beads (Qiagen) for 4 h at 4 °C. After washing, Ni-NTA beads (Qiagen) with 200 ml buffer containing 500 mM NaCl, 50 mM Tris pH 7.5, 0.5 mM TCEP, 25 mM imidazole and 5% glycerol. The protein was eluted with buffer containing 500 mM NaCl, 50 mM Tris pH 7.5, 0.5 mM TCEP, 250 mM imidazole and 5% glycerol. The eluted protein was then gel filtered on a Superdex-200 10/300 GL size-exclusion column (GE Life Sciences) in buffer containing 500 mM NaCl, 50 mM Tris pH 7.5, 0.5 mM TCEP and 5% glycerol. The desired fractions were collected and concentrated using Amicon Ultra-4 Centrifugal Filter Units with 3 kDa cut-off. HP1α, pHP1α[5] and xAurora-B–INCENP$^{790-856}$ (ref. [47]) were expressed and purified as previously described. GFP was expressed from a pET28a-GFP vector in BL21(DE3)pLysS cells. Cells were lysed in PBS containing 0.5 mM TCEP and 5 mM imidazole and purified using Ni-NTA beads (Qiagen). After washing with PBS supplemented with 0.5 mM TCEP and 25 mM imidazole, GFP was eluted in PBS supplemented with 0.5 mM TCEP and 250 mM imidazole. GFP was then dialysed in PBS supplemented with 0.5 mM TCEP. GFP–xMad2 was generated by cloning the gene encoding 6×His–eGFP onto the N terminus of *Xenopus* Mad2 in pET28a vector and the protein was then purified from *E. coli* on Ni^{2+}-Agarose.

h*SGO1*$^{1-112}$ was cloned into pMCSG17 containing an N-terminal 6×His+MBP-tag to obtain a pMCSG13-6×His-MBP-hSGO1$^{1-112}$ construct with a TEV cleavage site between MBP and h*SGO1*$^{1-112}$. BL21(DE3)pLysS cells containing pMCSG13-6×His-MBP-hSGO1$^{1-112}$ were grown to an OD of 0.8 and recombinant protein expression was induced using 0.3 M IPTG at 18 °C for 16–18 h. The cells were then collected and lysed in buffer containing 150 mM NaCl, 20 mM Tris pH 7.5, 0.5 mM TCEP, 5% glycerol, 5 mM imidazole and protease inhibitor cocktail (Roche) using an EmulsiFlex-C3 homogenizer. The lysate was incubated with Ni-NTA beads (Qiagen) for 4 h at 4 °C. The beads were then washed with buffer containing 150 mM NaCl, 20 mM Tris pH 7.5, 0.5 mM TCEP, 5% glycerol and 25 mM imidazole. The protein was then eluted with buffer containing 150 mM NaCl, 20 mM Tris pH 7.5, 0.5 mM TCEP, 5% glycerol and 250 mM imidazole. The 6×His-MBP tag was then cleaved from the protein during dialysis with TEV protease in buffer containing 150 mM NaCl, 20 mM Tris pH 7.8, 0.5 mM TCEP and 5% glycerol. Gel filtration for the resulting cleaved protein was then performed using a Superdex-200 10/300 GL size-exclusion column (GE Life Sciences) in buffer containing 150 mM NaCl, 20 mM Tris pH 7.5, 0.5 mM TCEP and 5% glycerol. The fraction containing hSGO1$^{1-112}$ was then further purified by ion-exchange chromatography using a HiTrap SP HP column (GE lifesciences) with a 75–500 mM KCl gradient. The purified hSGO1$^{1-112}$ protein was collected and stored at −80 °C.

Phase-separation assay. Phase separation was induced by diluting the indicated amount of ISB in the low salt buffer (50 mM Tris pH 7.5 and 1 mM dithiothreitol (DTT)) to achieve the indicated final concentration of protein and NaCl. To induce phase separation in the presence of a molecular crowding agent, ISB at the indicated concentration was incubated in buffer containing 5% PEG-3350, 50 mM Tris pH 7.5, 1 mM DTT and the indicated amount of NaCl. The indicated concentration of 2×-α-satellite DNA, histone H3.3 polynucleosome (containing 12 nucleosomes; active motif), 2×-α-satellite RNA or paclitaxel-stabilized microtubules was incubated with 8 μM ISB in buffer containing 150 mM NaCl, 50 mM Tris pH 7.5 and 1 mM DTT. Phase separation was observed by adding a drop of the reaction onto the coverslip and then imaging the ISB droplet using a ×63 objective on a Zeiss Observer Z1 wide-field microscope by fluorescence and DIC imaging, or using a JEOL 1230 for transmission electron microscopy. For time-lapse imaging of ISB droplet fusion, ISB droplets were formed in the indicated conditions and immediately imaged under DIC every second.

Partitioning of constituents into ISB coacervates. ISB coacervates were generated by incubating 5–6 μM ISB in buffer containing 150 mM NaCl, 50 mM Tris pH 7.5, 1 mM DTT and 5% PEG-3350. Then, 400 nM (unless otherwise stated) of the indicated agent molecules were incubated with ISB coacervates for 2 min at room temperature and imaged immediately. To calculate the partition coefficients for the histone peptides, the ISB coacervates were generated by incubating 20 μM of ISB in buffer containing 150 mM NaCl, 50 mM Tris pH 7.5, 1 mM DTT. Fluorescence signals were calculated using Volocity (v.6.3, PerkinElmer). Partition coefficients were calculated by dividing the fluorescence signal per unit area inside the coacervates by the fluorescence signal per unit area outside the coacervates after subtracting the background fluorescence. Background fluorescence was calculated by imaging the coacervates in the absence of fluorescent agent molecules.

Unmodified histone H3 or H3pT3 synthetic peptides (ARTKQTARKSTGGKAPRKQLY–fluorescein (note the additional tyrosine, to enable concentration measurement at 280 nm, and C-terminal fluorescein); (GenScript) were previously described[13]. Then, 400 nM rhodamine-labelled α/β-tubulin dimers (Cytoskeleton), 400 nM HP1α–CF555, 1 μM hSGO1$^{1-112}$–CF555, 100 nM xAurora-B–xINCENP$^{790-856}$–CF555, 400 nM Cy3–2×-α-satellite DNA, 400 nM 2×-α-satellite RNA, 400 nM Cy3-azide, 400 nM GFP and 400 nM GFP–xMad2 were incubated with phase-separated ISB coacervates. 2×-α-satellite RNA was generated by in vitro transcription of the 2×-α-satellite-DNA PCR product, which was amplified from a vector containing the 2×-α-satellite-DNA sequence (a gift from D. Foltz) using primers containing the T7 transcription initiation sequence (forward: TAATACGACTCACTATAGGGAGAAAGTGGATATACAGACCCC; reverse: TCCACTTGCAGACTTTACAAACAG). In vitro transcription was carried out using the Megascript T7 Transcription Kit (Thermo Fisher) spiked with Cy3–UTP, RNA was then treated with DNase and isolated using the RNA Clean and Concentrator Kit (Zymo Research). Cy3–2×-α-satellite-DNA was generated by PCR and spiked with Cy3–dCTP; we used the primers listed above and purified the product by gel extraction. HP1α, hSGO1$^{1-112}$ and xAurora-B–xINCENP$^{790-856}$ were labelled with Mix-n-Stain CF555 labeling kit (Sigma-Aldrich) according to the manufacturer's protocol followed by dialysis to remove unreacted dye molecules.

Measurement of saturation concentration using a spin-down method. ISB alone or mixed with other indicated proteins was incubated in buffer containing 150 mM NaCl, 50 mM Tris pH 7.5 and 0.5 μM TCEP to induce phase separation in a 15 μl reaction. The reaction was allowed to stand for 5 min and then centrifuged at 16,100*g* for 10 min to separate the soluble phase from the droplet phase. Then, 5 μl from the top phase was removed and analysed using SDS–PAGE to determine the saturation concentration. The same concentration of ISB that was used in the reaction was also added to buffer with a high concentration of salt to prevent phase separation and a serial dilution of this solution was loaded onto the same gel along with the top phase of spun-down phase-separated solution to create a standard curve (often with coefficient of determination $R^2 > 0.99$), which was used to accurately determine the saturation concentration of ISB. The SDS–PAGE gel was stained with GelCode Blue (Biorad) according to the manufacturer's protocol and subjected to densitometry using ImageJ. For experiments shown in Fig. 4d, 15 μM ISB was incubated with equimolar concentrations of the indicated proteins in buffer containing 150 mM NaCl, 50 mM Tris pH 7.5 and 0.5 μM TCEP. For experiments shown in Fig. 4e, 40 μM ISB was incubated with 10 units of CDK1/Cyclin B (Enzo, BML-SE128-0100) in buffer containing 5 mM Tris pH 7.5, 300 mM NaCl, 0.1 mM DTT, 5% glycerol, 50 mM HEPES, 10 mM $MgCl_2$, 1.1 mM EGTA, 0.011% Brij-35, 0.5 μM TCEP and 1 mM ATP (ATP or CDK1/Cyclin B was left out for the indicated condition and replaced with their respective dissolving buffer) for 1.5 h at room temperature. Phase separation was then induced by lowering the NaCl concentration to 150 mM by diluting the reaction mixture twofold with buffer containing 50 mM Tris pH 7.5 and 0.5 μM TCEP followed by centrifugation and gel analysis as described above.

Microtubule preparation and microtubule-dependent phase separation. Paclitaxel-stabilized microtubules were prepared by polymerizing bovine-brain tubulin dimers spiked with rhodamine-labelled α/β-tubulin dimers in BRB80 (80 mM PIPES, 1 mM $MgCl_2$, 1 mM EGTA, pH 6.8 with NaOH), 1 mM DTT and 1 mM GTP with an increasing concentration of paclitaxel; paclitaxel-stabilized MTs were then separated from the unpolymerized tubulin dimers by centrifugation through a 40% glycerol cushion at 137,000*g*. Then, 6 μM GFP–ISB was incubated with 1 μM paclitaxel-stabilized rhodamine-MTs in buffer containing 50 mM Tris pH 7.5, 150 mM NaCl, 1 mM DTT and 20 μM paclitaxel for 15 min at room temperature. A drop of the reaction was placed between coverslips and imaging was performed at ×63 using a Zeiss Observer Z1 wide-field microscope.

Cell culture and stable cell-line generation. HeLa T-REx cells (ThermoFisher Scientific) and HeLa Kyoto cells with endogenously tagged INCENP–mCherry and Aurora-B–GFP (a gift from J. Ellenberg)[29] were grown in Dulbecco's modified Eagle's medium (DMEM; Invitrogen) supplemented with 10% fetal bovine serum (Gibco). U2OS-LacO-TRE cells were grown in DMEM-Glutamax medium (Gibco). All of the cells were grown in the presence of 5% CO_2 in a humidified incubator at 37 °C.

To generate HeLa T-REx cells stably expressing LAP–borealin^{WT} and LAP–borealin$^{\Delta 139-160}$, the borealin^{WT}-transgene fragments were sub-cloned into the pCDNA5/FRT vector (Invitrogen) containing an N-terminal LAP-tag sequence. LAP–borealin$^{\Delta 139-160}$ was generated by deleting the region coding for borealin residues 139–160 by site-directed mutagenesis. LAP–borealin^{8A} and LAP–borealin^{13A} were created by sub-cloning gBlocks (IDT) containing the sequences of borealin^{8A} and borealin^{13A} in a pCDNA5/FRT vector (Invitrogen) containing an N-terminal LAP-tag sequence. The resulting LAP–borealin^{WT}, LAP–borealin^{8A}, LAP–borealin^{13A} and LAP–borealin$^{\Delta 139-160}$ plasmids were co-transfected with the pOG44 plasmid (Invitrogen) using Lipofectamine 2000 (Invitrogen). Cells were subjected to selection for 15 d in the presence of 200 μg ml^{-1} hygromycin B (Invitrogen). To obtain cells with homogenous expression of the transgenes,

selected colonies were pooled and FACS sorted for expression of GFP (for LAP–borealin transgenes).

Plasmid and siRNA transfection. Plasmid transfection was performed using Lipofectamine 2000 (Invitrogen) according to the manufacturer's protocol.

For knockdown and replacement experiments, borealin 3′ UTR siRNA (AGGUAGAGCUGUCUGUUCAdTdT)[25] was transfected using RNAiMAX (Invitrogen) according to the manufacturer's protocol. To analyse mitotic phenotypes in the first mitosis after complementation, borealin stable cell lines were plated in the presence of 2 mM thymidine. Then, 24 h after plating, cells were added to fresh medium and transfected with siRNA. Another round of siRNA transfection was performed after 12 h of the first round of siRNA treatment and 2 mM thymidine was added. After 12–14 h of the second round of siRNA treatment, cells were released from thymidine in fresh media. For immunofluorescence analysis, cells were fixed after 8–10 h; for live-cell imaging, cells were treated as indicated.

Live-cell imaging. For live-cell imaging, cells were plated in a 4-well imaging chamber (Labtek) in the presence of 2 mM thymidine followed by treatment with siRNA. Then, 3–4 h after the second thymidine release, 200 nM SiR-DNA (Cytoskeleton) dye was added to the cells; 1.5 h after SiR-DNA treatment, time-lapse images were taken for 16 h at 5 min intervals using a Zeiss Observer-Z1 in a humidified chamber maintained at 37 °C in the presence of 5% CO_2. Videos were analysed using Volocity software (v.6.3; PerkinElmer).

FRAP analysis. GFP–ISB coacervates were generated by incubating 6 µM GFP–ISB in buffer containing 150 mM NaCl, 50 mM Tris pH 7.5, 1 mM DTT and 5% PEG-3350 supplemented with oxygen-scavenging solution containing 40 mM glucose, 130 mg ml^{-1} glucose oxidase and 24 mg ml^{-1} catalase. GFP–ISB coacervates were then placed in a flow chamber constructed by placing two strips of double-sided tape on a coverslip and placing a second coverslip on top of it to form a grove. FRAP experiments were performed using a Zeiss 880 confocal microscope by acquiring 2 time points before bleaching and then bleaching with 20 cycles of 488 nm laser at 100% power and imaging every 1.5 s for 265 s. Fluorescence intensities were measured using Volocity (v.6.3, PerkinElmer). Recovered intensity corrected for photobleaching that occurred due to imaging was termed as the percentage-corrected recovered intensity (Nt) and was calculated using the following equation at each time point.

$$Nt = \left\{ \frac{\left[\left(\mathrm{Ft} - \mathrm{F0}_{\mathrm{postbleach}}\right)/\mathrm{Ft}_{\mathrm{unbleached}}\right]}{\left[\left(\mathrm{F0}_{\mathrm{prebleach}} - \mathrm{F0}_{\mathrm{postbleach}}\right)/\mathrm{F0}_{\mathrm{unbleached}}\right]} \right\} \times 100$$

Where,

Ft, fluorescence intensity at time (t).

$F0_{postbleach}$, fluorescence intensity immediately after bleaching.

$Ft_{unbleached}$, fluorescence intensity at time (t) of unbleached coacervate.

$F0_{prebleach}$, fluorescence intensity before bleaching.

$F0_{unbleached}$, fluorescence intensity of unbleached coacervate at the same time as $F0_{prebleach}$.

The graph of Nt versus time was fitted with a one-phase association equation with a least-squares fitting method using Prism software (GraphPad; green, Fig. 2a). The mobile fraction and $t_{1/2}$ with 95% confidence intervals were extracted from this curve using Prism software (GraphPad).

FCS analysis. All of the in vivo FCS measurements were performed using a Zeiss LSM 880 microscope equipped with the quasar spectral array of a 32 GaAsP detector, an argon laser (Melles-Griot) set at 488 nm excitation and a Zeiss Plan-Apochromat ×63 1.2 NA DIC M27 oil-immersion objective. The acquisition modality was set with a sampling time of 0.2 µs, the laser power was set at 0.1% and a pinhole of 90 a.u. was used. Correlation curves were obtained by acquiring intensity fluctuations for 30 s, then the correlation curves were computed using ZEN Black Zeiss software. An image of the FCS spot was taken before and after recording the FCS trace to evaluate whether the cell underwent any movement or conformational change.

For live-cell FCS, HeLa TReX cells stably expressing GFP–borealin were plated on a 35 mm imaging petri dish and were allowed to grow overnight. Cells were then incubated for 1 h with 3.3 µM of nocodazole and stained with 20 µl of NucBlue (Thermofisher Scientific) diluted in 2 ml of cell culture medium. Cells were incubated during the imaging at 37 °C and 5.1% CO_2. Many cells in mitosis and interphase were chosen. For mitotic cells, FCS was carried out in the same cells at the inner-centromere region and in the cytoplasm. For cells in interphase, FCS data were acquired only inside the nucleus.

All FCS measurements of the in vitro GFP–ISB coacervates were carried out using a Zeiss LSM 510 microscope equipped with ConfoCor3 single photocounting photodiodes (SAPD), an argon laser set at 488 nm excitation and a ×40 water-immersion C-Apochromat NA 1.2 Zeiss objective. GFP–ISB coacervates were generated by incubating 5 µM of GFP–ISB with 15 µM of ISB in buffer containing a final concentration of 150 mM NaCl, 50 mM Tris pH 7.5 and 0.5 µM DTT. GFP–ISB coacervates solutions were then placed in a flow chamber constructed by two coverslips. The acquisition modality was set with a sampling time of 0.2 µs per time point and a pinhole of 100 a.u. GFP–ISB FCS are recorded centrally for many droplets and in solution to measure the diffusion coefficients of the proteins that were not phase separated (5 µM in 200 mM NaCl, 50 mM Tris pH 7.5 and 0.5 µM DTT).

All of the correlation curves were obtained by acquiring fluorescence-intensity fluctuations over 30 s, and were then computed using Zeiss LSM software. Correlation plots were fitted using two-populations (in live cells) and one-population models (in vitro) using SimFCS (Laboratory for Fluorescence Dynamics; www.lfd.uci.edu) as described previously[48,49]. FCS fitting parameters were obtained using the same settings of the experiment measuring FCS of eGFP as reported previously[50].

optoDroplet assay. Plasmids containing mCherry-*Cry2* were obtained from Brangwynne Lab[37], mCherry-*Cry2* was PCR amplified and cloned into pCDNA5-borealin vectors. pCDNA5 containing mCherry-*Cry2*, borealin^{WT}-mCherry-*Cry2* and borealin$^{\Delta 139-160}$-mCherry-*Cry2* were transfected in HeLa TREx cells 24 h after plating into a 4-well imaging chamber (Labtek). Constructs were allowed to express for 9–10 h. The cells were then imaged using a Zeiss Observer-Z1 in a humidified chamber maintained at 37 °C in the presence of 5% CO_2. Cells with similar expression levels of exogenous proteins were selected on the basis of mCherry intensity. To induce phase separation, cells were exposed to 488 nm wavelength light every 5 s and single z-plane images were taken in the 568 nm channel to observe focus formation. Quantification was performed using Volocity software (v.6.3, Perkin Elmer) by manually encircling foci at the 95 s timepoint to measure intensity per unit area in the foci. Enrichment of mCherry in the foci was quantified by calculating the ratio of intensity per unit area of the foci to that of an area near but not overlapping a focus (Supplementary Fig. 5a). Statistical analysis was performed using Prism (GraphPad).

LacO array experiment. U2OS-LacO-TRE cells containing 200 copies of 256×LacO/96×TRE arrays integrated in Chromosome 1[51] were plated in a 4-well imaging chamber (Labtek). Cells were imaged live using the DIC and mCherry channel 24 h after transfection with a pDF287 plasmid containing either LacI-mCherry alone or LacI-mCherry-borealin. The DIC signal at the region with differential refractive index is characterized by the presence of a dark area (low-intensity region) and a bright area (high-intensity region) adjacent to each other, yielding a characteristic horizontal S shaped profile that lies over the mCherry signal in our experiments. The DIC and mCherry signal was quantified by measuring intensities along a line (cyan arrow, Supplementary Fig. 5b) using ZEN Black Zeiss software. The direction of the line was chosen to go from the darkest to brightest area of the DIC foci. When no DIC foci were observed, the direction was chosen on the basis of the DIC signal of the nearby nuclear bodies. To control for variation in background intensities between images, the line profiles were normalized to the intensities of the first pixel that was outside a focus.

Mitotic chromosome spreads. We added 100 ng ml^{-1} KaryoMAX Colcemid (Gibco) to HeLa Kyoto cells expressing endogenously tagged INCENP–mCherry and Aurora-B–eGFP for 2 h. Mitotic cells were collected by mitotic shake-off, spun down and resuspended in a hypotonic buffer (25 mM KCl, 0.27% sodium citrate in distilled water) for 20 min at 37 °C. Swollen cells were then broken open and chromosomes were spread on coverslips using a Cytospin 4 (ThermoShandon). The coverslip was then transferred to the indicated buffer (20 mM HEPES, 5 mM $MgCl_2$, 25 mM NaCl or 220 mM NaCl, 0% or 10% PEG-3350, 1 mM DTT, 20 mM β-glycerophosphate and 1× protease inhibitor cocktail (Roche)) for 5 min and washed once more with the same buffer. The chromosomes were then fixed with 2% paraformaldehyde (PFA) in PBS for 15 min. The chromosomes were then stained with DAPI and mounted on a slide for imaging. Chromosomes were imaged at ×63 using a Zeiss Observer-Z1. The intensity of INCENP–mCherry and DAPI were quantitated at the inner centromere using Volocity (v.6.3, PerkinElmer). These values were plotted using Prism software (GraphPad) and the indicated statistical tests were applied.

Immunofluorescence microscopy. Cells were seeded on poly-L-Lysine (Sigma) coated coverslips and treated as indicated. Cells were then fixed with 4% paraformaldehyde in PHEM buffer (25 mM HEPES, 60 mM PIPES, 10 mM EGTA and 4 mM $MgCl_2$, pH 6.9) containing 0.5% Triton X-100 for 20 min at room temperature. After three washes with Tris-buffered saline (TBS), cells were blocked for 1 h with 3% BSA in TBS-T (TBS and 0.1% Tween-20) at room temperature. Cells were then incubated with primary antibodies in 3% BSA in TBS-T for 1 h at room temperature. Cells were then washed three times with TBS-T (10 min each) and incubated with fluorescent secondary antibodies (1:2,000; Jackson Immuno-Research). Cells were then washed four times with TBS-T and stained with 0.5 µg ml^{-1} DAPI for 5 min before being mounted on slides using ProlongGold antifade (Invitrogen) and sealed with nail polish. Image acquisition was performed as described previously[52]. Image processing and analysis was performed using Volocity (v.6.3, PerkinElmer). To quantify fluorescence levels at centromeres, we used an intensity thresholding algorithm to mark all of the centromeres on the basis of ACA intensity. To eliminate changes in fluorescence intensity owing to

differences in centromere size, the total fluorescence intensity was divided by the total volume of the selected area. Background intensity was subtracted and the intensity/volume of the desired channel was normalized to the corresponding ACA intensity/volume. For quantification of Aurora-B intensity at the spindle midzones, the area in the furrow showing Aurora-B intensity was selected manually on a maximum-intensity-projection image of anaphase cells, and the sum of the intensity inside the selected area was measured. The sum of the intensity was divided by area to normalize the difference in area of selected regions. A region away from the spindle midzone was selected as background and intensity/area of this region was subtracted from that of the spindle midzones. Normalized intensity throughout the paper refers to normalized intensity with respect to the intensity of control cells or of cells expressing LAP–borealin^{WT}. The final normalized intensity values were plotted and analysed using Prism (GraphPad) and the indicated statistical tests were applied. For Fig. 5c,d, Aurora-B intensity at the inner centromere was measured by encircling the region between ACA lobes, and Aurora-B intensity on the chromosome arm was measured by selecting a region of similar dimensions that was adjacent to, but not between, ACA lobes on the chromosome arms. The sum of the intensity was divided by the volume of the selected region and the background intensity/volume was subtracted from it. The background intensity was determined by selecting a region away from the chromatin. The ratio of Aurora-B intensity/volume at the inner centromere to the ratio of Aurora-B intensity/volume on the chromosome arm was plotted. For Fig. 5e,f, Aurora-B intensity/volume at the inner centromere was measured by drawing a region of interest between two CENP-T spots, encircling the inner centromere. Background intensity/volume was determined by selecting a region of interest away from the inner centromere and was subtracted from the intensity/volume measured at the inner centromere. Most of the primary antibodies used in this study were obtained from commercial sources and are listed in Supplementary Table 1 with the exception of anti-borealin[52] and anti-CENP-T[53] antibodies, which have been described previously.

Statistics and reproducibility. All of the key experiments were repeated multiple times as indicated in the figure legends. For example, Figs. 1b–f, 2a–e, 3a–g, 4a–e, 6d and 7b,c were all performed independently at least three times with similar results. Experiments for Figs. 5a–h, 6c,f–k and 7e,f were performed twice independently. Indicated statistical analysis was performed using Prism (v.5, GraphPad). Where box and whisker plots are used, the middle line indicates median, the box indicates the 25–75th percentiles and the whiskers indicate the 5–95th percentiles.

Reporting Summary. Further information on research design is available in the Nature Research Reporting Summary linked to this article.

Data availability

Source data for Figs. 1–7 and Supplementary Figs. 1–7 are provided in Supplementary Table 2. The data that support the findings of this study are available from the corresponding author on reasonable request.

References

47. Rosasco-Nitcher, S. E., Lan, W., Khorasanizadeh, S. & Stukenberg, P. T. Centromeric aurora-B activation requires TD-60, microtubules, and substrate priming phosphorylation. *Science* **319**, 469–472 (2008).
48. Cardarelli, F., Lanzano, L. & Gratton, E. Fluorescence correlation spectroscopy of intact nuclear pore complexes. *Biophys. J.* **101**, L27–L29 (2011).
49. Moens, P. D. J., Gratton, E. & Salvemini, I. L. Fluorescence correlation spectroscopy, raster image correlation spectroscopy, and number and brightness on a commercial confocal laser scanning microscope with analog detectors (Nikon C1). *Microsc. Res. Tech.* **74**, 377–388 (2011).
50. Scipioni, L., Lanzanó, L., Diaspro, A. & Gratton, E. Comprehensive correlation analysis for super-resolution dynamic fingerprinting of cellular compartments using the Zeiss Airyscan detector. *Nat. Commun.* **9**, 5120 (2018).
51. Janicki, S. M. et al. From silencing to gene expression: real-time analysis in single cells. *Cell* **116**, 683–698 (2004).
52. Banerjee, B., Kestner, C. A. & Stukenberg, P. T. EB1 enables spindle microtubules to regulate centromeric recruitment of aurora B. *J. Cell Biol.* **204**, 947–963 (2014).
53. Sathyan, K. M., Fachinetti, D. & Foltz, D. R. α-Amino trimethylation of CENP-A by NRMT is required for full recruitment of the centromere. *Nat. Commun.* **8**, 14678 (2017).

nature research

Corresponding author(s): Peter Todd Stukenberg

Last updated by author(s): Jul 3, 2019

Reporting Summary

Nature Research wishes to improve the reproducibility of the work that we publish. This form provides structure for consistency and transparency in reporting. For further information on Nature Research policies, see Authors & Referees and the Editorial Policy Checklist.

Statistics

For all statistical analyses, confirm that the following items are present in the figure legend, table legend, main text, or Methods section.

n/a	Confirmed	
☐	☒	The exact sample size (*n*) for each experimental group/condition, given as a discrete number and unit of measurement
☐	☒	A statement on whether measurements were taken from distinct samples or whether the same sample was measured repeatedly
☐	☒	The statistical test(s) used AND whether they are one- or two-sided *Only common tests should be described solely by name; describe more complex techniques in the Methods section.*
☐	☒	A description of all covariates tested
☐	☒	A description of any assumptions or corrections, such as tests of normality and adjustment for multiple comparisons
☐	☒	A full description of the statistical parameters including central tendency (e.g. means) or other basic estimates (e.g. regression coefficient) AND variation (e.g. standard deviation) or associated estimates of uncertainty (e.g. confidence intervals)
☐	☒	For null hypothesis testing, the test statistic (e.g. *F*, *t*, *r*) with confidence intervals, effect sizes, degrees of freedom and *P* value noted *Give P values as exact values whenever suitable.*
☒	☐	For Bayesian analysis, information on the choice of priors and Markov chain Monte Carlo settings
☒	☐	For hierarchical and complex designs, identification of the appropriate level for tests and full reporting of outcomes
☒	☐	Estimates of effect sizes (e.g. Cohen's *d*, Pearson's *r*), indicating how they were calculated

Our web collection on statistics for biologists contains articles on many of the points above.

Software and code

Policy information about availability of computer code

Data collection	Volocity(V6.3, PerkinElmer), ZEN software 2012(Zeiss), Zeiss LSM software (Version 4.2 SP1).
Data analysis	ImageJ (Version 10.2), Volocity(V6.3, PerkinElmer), ZEN software 2012 (Zeiss), Prism (Version 5.0c) (GraphPad), SimFCS (Version 4) (the Laboratory for Fluorescence Dynamics), ZEN Black 2.3 SP1 software (V14.0) (Zeiss), .

For manuscripts utilizing custom algorithms or software that are central to the research but not yet described in published literature, software must be made available to editors/reviewers. We strongly encourage code deposition in a community repository (e.g. GitHub). See the Nature Research guidelines for submitting code & software for further information.

Data

Policy information about availability of data

All manuscripts must include a data availability statement. This statement should provide the following information, where applicable:

- Accession codes, unique identifiers, or web links for publicly available datasets
- A list of figures that have associated raw data
- A description of any restrictions on data availability

The data that support the findings of this study are available from the corresponding author upon reasonable request.

Field-specific reporting

Please select the one below that is the best fit for your research. If you are not sure, read the appropriate sections before making your selection.

☒ Life sciences ☐ Behavioural & social sciences ☐ Ecological, evolutionary & environmental sciences

Life sciences study design

All studies must disclose on these points even when the disclosure is negative.

Sample size	Sample size were chosen based on prior knowledge for obtaining significant p-values from the type of experiment performed.
Data exclusions	No data were excluded
Replication	All attempts at replication were successful. Number of times each experiment was repeated is stated in the figure legends. The FPLC profile shown in supplementary figure 1a, b are only performed once since these are traditionally only performed once per protein prep. For supplement figure 6 a-c, the western blots for this exact combination was performed only once although the siRNA knockdown of Borealin and expression of the trans-gene was assessed multiple times with these cells in different combinations. The localization of the CPC at the inner-centromere in cells expressing the phase-separation mutant was performed 3 times although the staining was done twice for Aurora B (fig. 6f,g) and once for INCENP (Supplement fig. 6d).
Randomization	Cells were randomly selected for imaging.
Blinding	No blinding was possible, since the same person performed and analyzed the data.

Reporting for specific materials, systems and methods

We require information from authors about some types of materials, experimental systems and methods used in many studies. Here, indicate whether each material, system or method listed is relevant to your study. If you are not sure if a list item applies to your research, read the appropriate section before selecting a response.

Materials & experimental systems

n/a	Involved in the study
☐	☒ Antibodies
☐	☒ Eukaryotic cell lines
☒	☐ Palaeontology
☒	☐ Animals and other organisms
☒	☐ Human research participants
☒	☐ Clinical data

Methods

n/a	Involved in the study
☒	☐ ChIP-seq
☒	☐ Flow cytometry
☒	☐ MRI-based neuroimaging

Antibodies

Antibodies used	Mouse monoclonal Aurora-B antibody (BD bisciences, Cat.no. 611083, lot no. 7346628, clone 6, 1 in 250 dilution); Rabbit polyclonal Borealin antibody (1 in 1000 dilution) (Stukenberg lab); Mouse monoclonal INCENP antibody (Abcam, cat.no. ab23956, Clone no.58-217 , lot no. GR17490-1, 1 in 1000 dilution); Human ACA antibody (Antibodies inc, Cat.no. 15-235, lot no. 441.23BK.95, 1 in 200 dilution); Rabbit polyclonal CENP-T antibody (Foltz lab, 1 in 1000 dilution); Rb polyclonal pH3T3 antibody (EMD millipore, cat. no. 07-424, lot no. 3012075, 1 in 2000 dilution); Rb polyclonal H2A pT120 antibody (Active motif, Cat. no. 61195, lot no. 31511001, 1 in 1500 dilution); Ms monoclonal Sgo1 antibody (Abcam, Cat. no. ab58023, lot no. GR263157-4, 1 in 100 dilution); Goat anti-Mouse IgG (H+L) Highly Cross-Adsorbed Secondary Antibody, Alexa Fluor 568 (Thermo Fisher Scientific, Cat.no. A11031, lot.no. 1736975, 1 in 2000 dilution); Goat anti-Rabbit IgG (H+L) Highly Cross-Adsorbed Secondary Antibody, Alexa Fluor 568 (Thermo Fisher Scientific, Cat.no. A11036, lot.no. 1832035, 1 in 2000 dilution); Donkey anti-Mouse IgG (H+L) Highly Cross-Adsorbed Secondary Antibody, Alexa Fluor 647 (Thermo Fisher Scientific, Cat.no. A31571, lot.no. 1757130, 1 in 2000 dilution); Alexa Fluor® 647 AffiniPure Donkey Anti-Human IgG (H+L) (Jackson ImmunoResearch laboratories Inc., Cat.no. 709-605-149, 1 in 2000 dilution); Peroxidase AffiniPure Donkey Anti-Rabbit IgG (H+L) (Jackson ImmunoResearch laboratories Inc., Cat.no. 711-035-152, 1 in 2000 dilution); Peroxidase AffiniPure Donkey Anti-Mouse IgG (H+L) (Jackson ImmunoResearch laboratories Inc., Cat.no. 715-035-150, 1 in 2000 dilution).
Validation	Mouse monoclonal Aurora-B antibody (BD bisciences, Cat.no. 611083, lot no. 7346628, clone 6) statement provided by manufacturer (Reactivity: Human (QC Testing) Mouse, Rat (Tested in Development)) (Application: Western blot (Routinely Tested) Immunofluorescence (Tested During Development)) http://www.bdbiosciences.com/us/reagents/research/antibodies-buffers/cell-biology-reagents/cell-biology-antibodies/purified-mouse-anti--aim-1-6aim-1/p/611083. Rabbit polyclonal Borealin antibody from stukenberg lab validated for reactivity to human Borealin by assessing localization and protein amount by immunofluorescence and western blotting following knockdown of the antigen (ref: PMID: 30737408, PMID: 24616220). Mouse monoclonal INCENP antibody (Abcam, cat.no. ab23956, Clone no.58-217 , lot no. GR17490-1) was validated by abcam : https://www.abcam.com/incenp-antibody-58-217-ab23956.html. Human ACA antibody (Antibodies inc, Cat.no. 15-235, lot no. 441.23BK.95) is derived from human CREST patient serum, which have autoimmune antibodies against centromere proteins, validation statement at the manufacturers website: https://www.antibodiesinc.com/products/centromere-protein?variant=12783211839547. Rabbit polyclonal CENP-T antibody (Foltz lab, 1 in 1000 dilution) was validated by IF staining and westernblotting following

knockdown of protein (ref: PMID: 28266506).
Rb polyclonal pH3T3 antibody (EMD millipore, cat. no. 07-424, lot no. 3012075) was validated by manufacturer: http://www.emdmillipore.com/US/en/product/Anti-phospho-Histone-H3-Thr3-Antibody,MM_NF-07-424.
Rb polyclonal H2A pT120 antibody (Active motif, Cat. no. 61195, lot no. 31511001) was validated by the manufacturer: https://www.activemotif.com/catalog/details/61195/histone-h2a-phospho-thr120-antibody-pab-1.
Mouse monoclonal Sgo1 antibody (Abcam, Cat. no. ab58023, lot no. GR263157-4) was validated by the manufacturer: https://www.abcam.com/shugoshin-antibody-ab58023.html.

Eukaryotic cell lines

Policy information about cell lines

Cell line source(s)	HeLa-TReX cells and U2OS-LacO cells were a gift from Dan Foltz Lab. HeLa Kyoto cells with endogenously tagged INCENP-mCherry and Aurora-B-GFP was a gift from Jan Ellenberg.
Authentication	HeLa-TReX cell lines were authenticated to be homogenous population of close derivative on HeLa cells by ATCC using STR analysis. HeLa-Kyoto cells were authenticated by STR analysis by Cell line services Gmbh,Germany.
Mycoplasma contamination	Cell lines were not tested for mycoplasma contamination.
Commonly misidentified lines (See ICLAC register)	No commonly misidentified cell lines were used in this study